EARTH SURFACE PROCESSES AND LANDFORMS
Earth Surf. Process. Landforms (2019)

Published online in Wiley Online Library
(wileyonlinelibrary.com) DOI: 10.1002/esp.4602

Geomorphological controls on fluvial carbon storage in headwater peatlands

D. M. Alderson,[1]* M. G. Evans,[1] J. J. Rothwell,[1] E. J. Rhodes[2] and S. Boult[3]
[1] Department of Geography, University of Manchester, UK
[2] Department of Geography, University of Sheffield, UK
[3] School of Earth and Environmental Sciences, University of Manchester, UK

Received 13 July 2018; Revised 18 February 2019; Accepted 21 February 2019

*Correspondence to: D. M. Alderson, Arthur Lewis Building, University of Manchester, Oxford Road, Manchester, UK, M13 9PL. E-mail: danielle.alderson@manchester.ac.uk

ESPL
Earth Surface Processes and Landforms

ABSTRACT: Geomorphological controls and catchment sediment characteristics control the formation of floodplains and affect their capacity to sequester carbon. Organic carbon stored in floodplains is typically a product of pedogenic development between periods of mineral sediment deposition. However, in organically-dominated upland catchments with a high sediment load, eroded particulate organics may also be fluvially deposited with potential for storage and/or oxidation. Understanding the redistribution of terrestrial carbon laterally, beyond the bounds of river channels is important, especially in eroding peatland systems where fluvial particulate organic carbon exports are often assumed to be oxidised. Floodplains have the potential to be both carbon cycling hotspots and areas of sequestration. Understanding of the interaction of carbon cycling and the sediment cascade through floodplain systems is limited.

This paper examines the formation of highly organic floodplains downstream of heavily eroded peatlands in the Peak District, UK. Reconstruction of the history of the floodplains suggests that they have formed in response to periods of erosion of organic soils upstream. We present a novel approach to calculating a carbon stock within a floodplain, using XRF and radiograph data recorded during Itrax core scanning of sediment cores. This carbon stock is extrapolated to the catchment scale, to assess the importance of these floodplains in the storage and cycling of organic carbon in this area. The carbon stock estimate for the floodplains across the contributing catchments is between 3482-13460 tonnes, equating on an annualised basis to 0.8-4.5% of the modern-day POC flux. Radiocarbon analyses of bulk organic matter in floodplain sediments revealed that a substantial proportion of organic carbon was associated with re-deposited peat and has been used as a tool for organic matter source determination. The average age of these samples (3010 years BP) is substantially older than Infrared Stimulated Luminesence dating which demonstrated that the floodplains formed between 430 and 1060 years ago. Our data suggest that floodplains are an integral part of eroding peatland systems, acting as both significant stores of aged and eroded organic carbon and as hotspots of carbon turnover. © 2019 The Authors. Earth Surface Processes and Landforms published by John Wiley & Sons Ltd.

KEYWORDS: Floodplain carbon storage; headwater peatland erosion; carbon cycling hotspots; floodplain geomorphology; Itrax core scanning

Introduction

As conveyors of organic and mineral sediment, water and contaminants, rivers play an instrumental role in landscape evolution, and their catchments feature a variety of depositional settings that can store sedimentological information about past and present sediment dynamics (Turner *et al.,* 2015). River systems and their associated landforms were traditionally considered as passive pipes of terrestrial organic carbon (OC), that would eventually be delivered to the ocean, but are now viewed as active sites of OC processing, redistribution and storage (Aufdenkampe *et al.,* 2011). Floodplains develop in the transition from erosion dominated to deposition dominated processes in the longitudinal profile of a river system (Figure 1), predominantly in lowland landscapes unconstrained by geology (Jain *et al.,* 2008). As major depositional landforms in river systems, floodplains are large carbon stores (Hoffmann *et al.,* 2009), but they are also sites of potentially high carbon mineralisation rates (Evans *et al.,* 2013) and so may act as hotspots of carbon processing.

Floodplain growth is geomorphologically controlled by the balance between lateral and vertical accretion, and erosional processes. Carbon in floodplains may accumulate as a component of sediment deposition, or as in-situ vegetation development. The delivery of OC-rich sediments to floodplains by overbank deposition from river channels, is estimated to be substantial, despite the fact that it has received relatively little attention (Cole *et al.,* 2007; Battin *et al.,* 2009; Tranvik *et al.,* 2009). This paucity of research stems from the absence of information on global floodplain extent, carbon cycling processes and flux magnitudes. Once organic-rich sediment is deposited or accumulated, floodplains (depicted in Figure 1 as multiple buried soils) have the capacity to act either as sources or sinks of carbon (Zehetner *et al.,* 2009) and importantly active

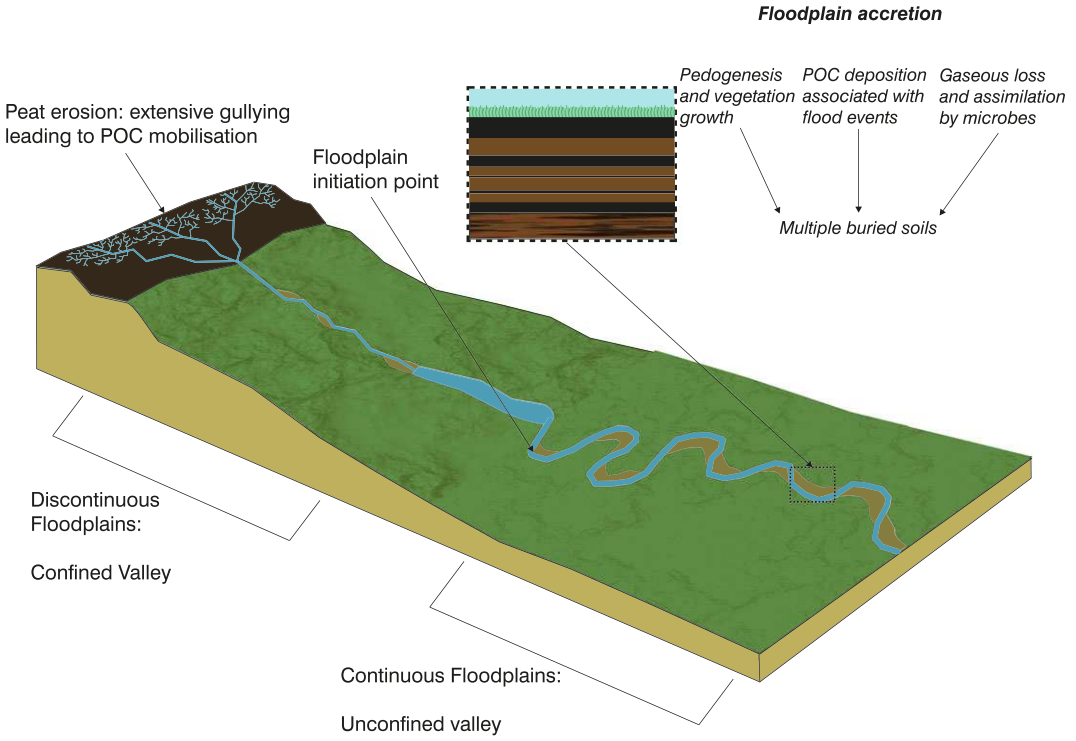

Figure 1. Carbon processing and storage in a peatland headwater catchment. [Colour figure can be viewed at wileyonlinelibrary.com]

hotspots of OM transformation (Hoffmann *et al.,* 2009; Zocatelli *et al.,* 2013).

The residence time and lability of OC in floodplains is controlled by geomorphological functioning and environmental conditions, including the height of the floodplain relative to average flood magnitude, grain size of sediments and succession of vegetation (Hoffmann *et al.,* 2013). For example, high energy, non-cohesive floodplains characterised by coarse sediments, limited vegetation coverage and substantial water table fluctuations are considered to have a low long-term storage potential of OC, because of the destructive and mobile nature of these channels, resulting in short residence times of deposited sediment and associated organics. Conversely, low energy, cohesive floodplains are often characterised by fine sediments, dense vegetation cover and infrequent water table fluctuations, and are more structurally stable in nature and therefore have a high long-term storage potential of OC.

In addition to geomorphological and environmental processes controlling absolute carbon storage potential, they may also control the balance of autochthonous versus allochthonous carbon accumulation. Allochthonous deposition is dependent on sediment load and character, in addition to the deposition processes during floods. Whereas pedogenesis is dependent on suitable conditions between floods, including the elevation of the floodplain from the river bed being high enough to allow suitable time for primary succession (Daniels, 2003; Bullinger-Weber *et al.,* 2014), and the frequency of high magnitude floods being sufficiently infrequent to rarely initiate overbank flow on the floodplain.

Some upland catchments in the UK are dominated by peat soils which have been subject to severe and widespread erosion (Evans *et al.,* 2006). As these soils are ~50% OC, the fluvial sediment yield from peatlands may be highly organic. Temporary headwater catchment storage by floodplains has been found to be particularly efficient during flood events (Evans and Warburton, 2005; Evans *et al.,* 2006). Floodplain deposition in headwater catchments below eroding peatlands potentially leads to high allochthonous input of carbon to the system and production of hotspots of carbon cycling, for example Evans *et al.* (2013) found that only 20% of POC deposited onto headwater floodplains was buried.

The fate of OC in floodplain landforms has previously received only minimal attention. Upland valleys with high sediment loads in particular may represent a critical point in the sediment cascade storing and processing OC from eroding organic-rich headwater sites. In this context, headwater peatland catchments with developed floodplains provide an ideal opportunity to explore the nature and characteristics of floodplain formation, development and carbon processing. The objectives of this paper are as follows: 1. Construct a geomorphological history of the formation and development of an upland floodplain in a highly organic catchment. 2. Quantify carbon storage in the floodplain and extrapolate this to the wider catchment. 3. Assess the relative importance of carbon source in the floodplain system. 4. Consider whether these systems are sites of carbon sequestration or turnover.

Geomorphological Context of the Study Area

This study will focus on floodplain systems in the southern Pennines, part of the Peak District National Park, in northern England. The extensive peatlands of the Peak District currently represent a net sink of 62 ktonnes of CO_2 equivalent per year (Worrall *et al.,* 2009). The River Ashop and River Alport drain the slopes of both Bleaklow and Kinder Scout; both upland plateaux which support an extensive cover of blanket peat. These are amongst the most severely eroded peatland sites in the UK (Evans and Lindsay, 2010), with a substantial POC flux derived from them (Pawson *et al.,* 2008; Pawson *et al.,* 2012). The peat erosion has occurred largely in the last 1000 years in response to pollution, land use pressures and climate change (Evans *et al.,* 2006). The River Ashop catchment is 38 km^2 (Pawson, 2008) whereas the River Alport catchment is 11 km^2. The catchments are underlain by interbedded sandstones and mudstones of the carboniferous age Millstone Grit series (Wolverson-Cope, 1976).

The peatlands in the study area are subject to characteristic pressures faced by many peatlands around the world including climatic, land use and pollution pressures (Holden *et al.,* 2007). The Peak District peatlands have been found to be particularly vulnerable as they are marginal to the climatic space suitable for growth of peat bogs in the UK (Clark *et al.,* 2010). They are therefore susceptible to future climate changes, which could result in further erosion and redistribution of these significant long-term carbon stores.

Continuous headwater floodplains are atypical in upland landscapes as the channel is confined and the landscape too steep for fine sediment to be regularly deposited beyond the boundaries of the channel. In the study area, regular, fine-grained, stable floodplains are present, despite the upland nature of the landscape. Floodplain development may be in part associated with gradient reductions associated with valley constrictions due to extensive Holocene landsliding in the region (Johnson and Walthall, 1979; Tallis and Johnson, 1980). Evidence for previous landslides in the specific area of investigation in this study can be observed in Figure 2, providing a reduction in gradient that has produced more lateral accommodation space for floodplain formation.

Understanding the role of floodplains in carbon storage and cycling in fluvial catchments that have characteristic high organic matter loads is twofold. Firstly, peatland carbon budget studies often assume oxidation of fluvial exports as standard practice. In the study area, previous research has focused on the geomorphological functioning, and carbon cycling within the peatlands themselves. However, less attention has been given to the off-site fate of eroded peatland carbon and to ascertain whether the assumptions regarding off-site oxidation are correct. The Ashop system is an extreme end-member where fluvial organic exports are particularly large as a result of acute erosion. By developing our understanding of how carbon is cycled through the landscape in this severely eroded system, we can enhance our understanding of the fate of peatland carbon exports more generally.

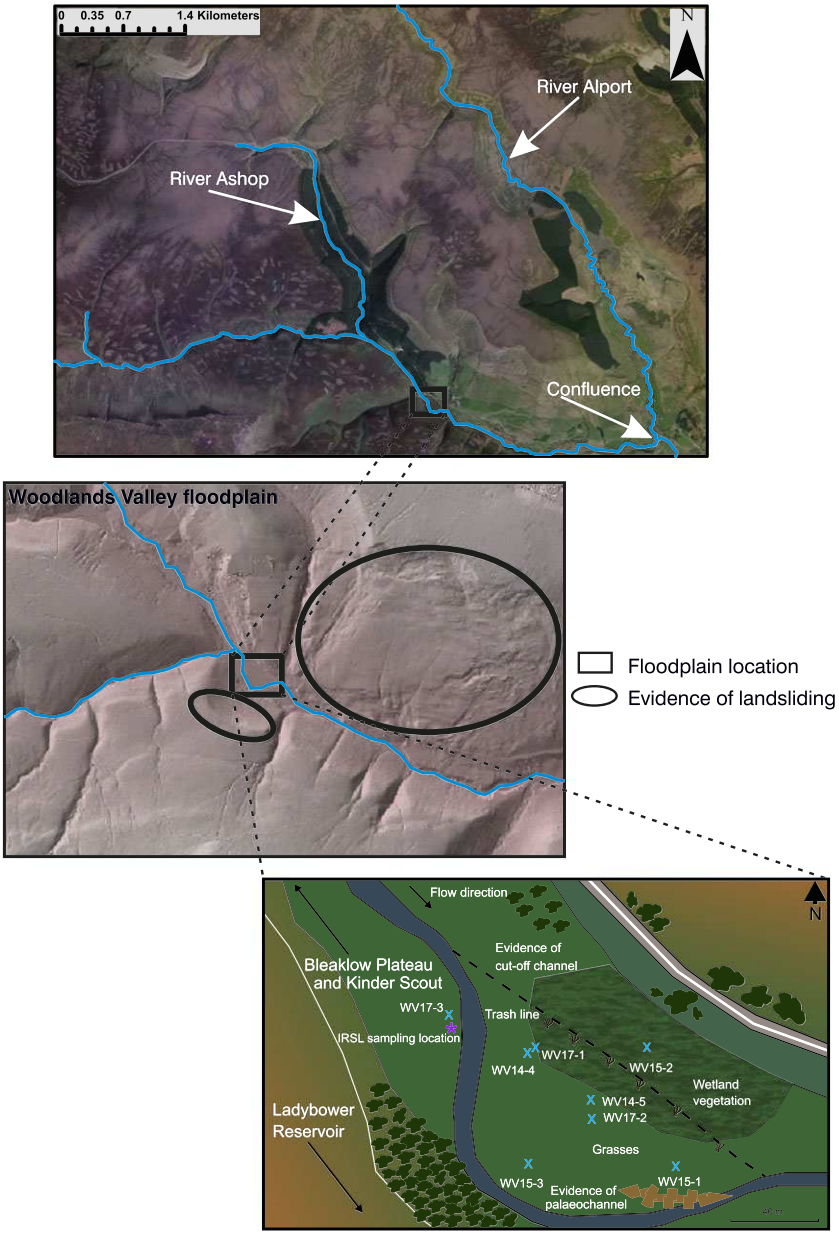

Figure 2. Location of the floodplain in relation to the River Ashop and River Alport. DEM evidence of landsliding along the River Ashop, Derbyshire, UK around the floodplain location. Coring locations: The majority of cores were taken on the large bar to the east. Only one core was taken on the west bar, but IRSL dates were also obtained from the bank of this bar. Topmost image: Imagery ©2019 Google, Map data ©2019 Google. [Colour figure can be viewed at wileyonlinelibrary.com]

Secondly, the nature and level of erosion of blanket peatlands in the UK at present is globally atypical, but peatlands that are currently sequestering carbon are at risk of losing this function as they are vulnerable to future climate change and land use pressures (Settele *et al.,* 2014; Bonn *et al.,* 2016). As such, more peatlands, and especially those in upland environments (Li *et al.,* 2017) are at risk of approaching the erosion status of the extreme end-member catchments in this study. This reinforces the importance of acquiring knowledge of the off-site fate of eroded fluvial carbon exports from peatlands.

Methods

Sample collection

Cores were collected across a floodplain reach of the upper Ashop (Woodlands Valley) where exposed sections indicated the presence of organics in the stratigraphy. Multiple floodplains of this nature are present along the reach, and this floodplain in particular was chosen for accessibility. To understand floodplain development and account for spatial variability of sediment distribution and type, sediment cores were collected from two core transects spanning a single meander bend on the floodplain of the River Ashop. The floodplain had clear evidence on the basis of visual imagery and an observed flood during the study period, of a previous palaeochannel and a present-day cut-off channel, only utilised during extreme floods (Figure 2). Two stands of vegetation with a distinctive border are present on the floodplain, with wetland-type vegetation towards the back of the floodplain, at the furthest point from the channel, and grasses present nearest the channel. Some of these modern-day features are key to interpreting the sediments within the floodplain.

Cores were collected in circular Perspex tubes using a Van Walt stitz corer in three sampling periods during 2014 (WV14-4 and WV14-5), 2015 (WV15-1, 2 and 3) and 2017 (WV17-1, 2 and 3) (Figure 2). WV17-1 and WV17-2 were taken as replicate cores to use for radiocarbon dating. Cores were transported in a horizontal position and refrigerated at 5°C. Immediately before scanning, the cores were split in half, with one half designated as the archive and prepared for core scanning.

Samples for IRSL (Infra Red Stimulated Luminescence) dating were collected from a bare face of the river channel on the west point-bar of the floodplain, close to the location of the core WV17-3 (Figure 2). Steel tubes were pushed into the cleaned sediment face and extracted, and a gamma spectrometer was used to measure the in-situ gamma dose rate. A sample of contemporary sediment was also collected from a small bar within the active channel at the same location using the method above.

Core scanning and correlation

All cores were scanned for optical imagery, X-radiography and micro-XRF using a Cox Analytical Systems Itrax core scanner with a step size of 200 microns for the entirety of each core. The XRF scans were completed using a molybdenum X-ray tube set at 55 kV and 30 mA with a count time of 15 seconds, which produces good excitation for a large range of elements of interest in geochemistry (Croudace *et al.,* 2006). Cores were covered with a 6 µm film to prevent dessication while running overnight and to avoid contamination of the XRF detector.

Instrument settings were optimised post-scan using the Cox Analytical Systems Q-Spec software to optimise the mathematical model by adjusting settings for the X-ray tube and detector parameters to ultimately reduce the mean square error (MSE) of the sum spectra. The enhanced fit was then used to re-evaluate all single spectra with a maximum of 20 iterations per spectrum using an automated batch procedure. Individual spectra with high MSE (generally >4) were then identified and the settings further altered as above to reduce MSE. The XRF spectra were quantified using the Q-spec software, producing results in peak area. Quantitative data is challenging to obtain because of the effects variations in water content, OM content and particle size may have on the diffraction of X-rays, and total count rate (Croudace and Rothwell, 2015).

Core correlation was a necessity for a geomorphological understanding of the floodplain processes but will only be successful in vertically accreting assemblages. Geochemical profiling is a robust method to link together layers with similar characteristics. The specific element that was used to achieve this was Pb, which is relatively immobile under variable water tables in comparison to other elements (Shuttleworth *et al.,* 2015), with a substantial body of literature devoted to the study of the behaviour, and increases in Pb content in the peat profile associated with industrial pollution and smelting (Lee and Tallis, 1973; Livett *et al.,* 1979).

Whilst Pb is the best element for core correlation, scanning sediment cores while wet has known limitations which may mean that results are an expression of water or OM content rather than actual variability in the element of interest. ICP-MS on a sub-set of samples from WV14-5 was used as validation to calibrate metal concentrations.

Sedimentology and grain size

Visual observation using the cores themselves, and the detailed optical imagery from the core scanner at a resolution of 47 microns, were used to produce sedimentological descriptions for each core containing information regarding contacts between different facies types, colour changes reflecting oxidation, and macrofossil presence.

Based on sedimentological interpretation (sharp erosional contacts with the layer below and flood couplets featuring coarsening up followed by fining up changes in mineral grain size), three layers from WV14-5 (380-465, 490-555 and 570-625 mm) interpreted to be single flood events were sampled. In addition, sediment deposited on the floodplain during a major flood event on the 21st November 2016 was sub-sampled to examine grain size relationships during a modern flood event. The grain size of the mineral component was measured using a Malvern 2000G laser granulometer at 0.5 cm intervals in the core samples, and at more irregular intervals in the modern sediments. Samples were treated with H_2O_2 to remove OM prior to measurement.

Developing a stratigraphic interpretation of organic source in headwater floodplain sediments

A selection of key criteria were developed as an initial aid to distinguish between in-situ soil growth and eroded overbank peat deposition on floodplains (Table I).

Floodplain sediments dominated by overbank deposition processes typically comprise of distinctive couplets, consisting of minerogenic sediment and an organic cap (Turner *et al.,* 2015). The organic cap of a flood couplet within floodplain

Table I. Factors determining allochthonous and autochthonous source in headwater floodplains in peatland catchments

Factor	In-situ soil	Eroded peat
Context in flood deposit	Thick organic layer on top of minerogenic flood unit	Thin organic layer on top of minerogenic flood unit
Root presence	Present and distinguishable but may become less so downcore when the material is more decomposed	Unlikely to have any distinguishable roots
Texture	Consolidated	Particulate
OC content	High	Lower

sediments downstream may represent both in-situ autochthonous accumulation and fluvially transported organics eroded from the peatlands, ultimately forming what may appear to be multiple buried soils. However, distinguishing between these two sources of OM is not straightforward, in large part as they are likely to be mixed in an individual organic horizon.

To aid in distinction of carbon source it is imperative to consider at what stage allochthonous organics associated with peat erosion would be laid down during a flood event. There is a scarcity of literature on organic transport and deposition on alluvial landforms during flood events, and therefore we interpret the likely sequence of events on the basis of changing energy conditions during the passage of the flood wave (Costa, 1978; Pizzuto *et al.,* 2008).

During the rising flood, organics are likely to be transported, but it is improbable that the floodwaters would be high enough to initiate overbank flow on the floodplain, and therefore they may simply be washed downstream. However, during the peak of the flood event, flow velocities both within the stream and on the floodplain, are likely to be sufficient to transport sediment. Any deposited sediment that did previously breach the channel bank may be scoured from the floodplain with other unconsolidated material at the surface. Evidence suggests that on frequently flooded alluvial landforms, litter is substantially reduced in comparison to no-flood zones (Saint-Laurent *et al.,* 2016). However, velocities may be such that floodplain residence times may not permit settling of organic matter. Therefore, the most likely time period for organics to settle, is during receding flows, when flow velocity is reduced, but flows remain high enough to continue to inundate the floodplain.

A key criterion in distinguishing between allochthonous and autochthonous layers is the context within the flood deposits and the thickness of an organic layer. Thicker organic layers containing fibrous material most likely contain a substantial proportion of organics as a result of pedogenic development (although they may also contain allochthonous material at the base), whereas thinner layers or lenses are more likely to relate to allochthonous peat deposition. The presence of roots in a suspected in-situ soil deposit provide good evidence that pedogenesis has taken place.

Carbon stock calculation

Core scanning offers the potential to calculate detailed carbon stocks with little laboratory preparation by using density and carbon content proxies from the data collected during a scan.

The Itrax core scanner can record high quality, high-resolution X-radiographic images (Francus *et al.,* 2015). Incident X-rays are attenuated by a wide range of phenomena, with grey levels acting as a measure of attenuation. The dominant control on beam attenuation is sediment thickness and bulk sediment density. The latter is influenced by various factors such as sediment porosity, water content, composition (OM, biogenic silica, mineralogy), and grain size (St-Onge *et al.,* 2007). Fortin *et al.* (2013) show that sediment density may be calculated using radiographic data for each pixel. The radiograph images obtained are 'radiographic positives', so that low-density areas appear light and higher density areas appear darker (Croudace *et al.,* 2006).

Between 18 and 20 subsamples (1 cm^3) were taken from each core, and wet and dry bulk densities calculated by weighing immediately post-sampling, followed by a repeat weighing after 24 hours in a furnace at 65°C. Radiograph imagery was analysed in Matlab producing an average value across each row. The greyscale value for each 200 μm increment was then averaged to the corresponding 1 cm depth interval for every increment in each core. Regression was performed between the Matlab-derived greyscale value from the X-radiograph, and actual dry bulk densities. Individual regression relationships were calculated for each core because the greyscale values may not be comparable between cores because of the variety of factors that determine sediment density.

Primary X-rays during XRF scanning produce two types of scattering. Rayleigh (or coherent) scattering leaves the photon energy unchanged, while Compton (or incoherent) scattering transfers some of the photon energy to electrons in the irradiated material, slightly lowering the energy of the photons. The amount and relative proportions of the different scattering mechanism varies with atomic number (Duvauchelle *et al.,* 1999). High OM content causes more scattering, and favours the Compton mechanism. The incoherent/coherent scattering ratio, may be used as an indicator of changes in OM and water content (Thomson *et al.,* 2006; Liu *et al.,* 2013). This ratio is an approximation of the atomic number of the average matrix composition. Incoherent scattering is known to be inversely related to the mean atomic number of the sediment (Croudace *et al.,* 2006). Higher intensities of incoherent scattering thus often reflect higher water and organic contents (Thomson *et al.,* 2006) and/or lower compaction (higher porosity) in the sediments of the topmost parts of the profile. Chawchai *et al.* (2016) in a study in Thailand, showed that the ratio has a strong correlation with LOI or TOC when a whole, lithologically variable sediment sequence is used.

To obtain C% values that could be directly compared to the Inc/Coh ratio, 19 dried sub-samples from WV14-5 were ground using a Fritsch vibratory Micro Mill Pulverisette 0 ball mill and prepared for CHN analysis using a Thermo Fisher Scientific Flash 2000 CHNS/O analyser to obtain C%. Three repetitions were run per sample, with calibration and standards run regularly to check the validity of the results. Inc/Coh ratios for the corresponding 1 cm interval for each sample were averaged to produce one value. Regression performed between the Inc/Coh value and the C% derived from the CHN analyser for just WV14-5 produced a very strong positive, significant correlation (n=19, R^2=0.75, p<0.01), so no further CHN analysis was completed for other cores.

The regression relationship between the Inc/Coh ratio and C% was used to derive a predicted carbon percentage for every

200 µm increment of scanned data, with associated standard error for every increment. Using the same method, dry bulk density for every increment was predicted with associated standard error using the relationship between the radiograph greyscale value and absolute dry bulk density. Predicted carbon proportion and dry bulk density were multiplied to obtain the amount of C in each 200 micron increment of core and added together to produce a total carbon stock for each core, accounting for volume. The errors associated with the predictions of carbon content and density were appropriately propagated.

$$CS = C \times D \times V \tag{1}$$

Total carbon stock (CS) was calculated according to Equation (1) where C is carbon content, D is density and V is volume. Errors were propagated appropriately throughout each stage of the calculation dependent on whether additive or multiplicative errors were needed. The errors associated with derived density and carbon content for each increment were calculated by adding the standard error of all values to the actual value.

$$E = \sqrt{\left(\frac{SEd}{d}\right)^2 + \left(\frac{SEc}{c}\right)^2} \tag{2}$$

Errors were then propagated for each increment according to Equation (2), where E is total error, SEd is standard error of predicted density, d is predicted density, SEc is standard error of predicted carbon and c is predicted carbon content. Furthermore, to calculate total error for each core, individual errors for each increment were additively propagated.

To account for spatial heterogeneity across the floodplain in sediment carbon concentrations, the carbon stock was calculated in each of the five locations representing different areas of the floodplain. The basal sediments from WV15-1, WV15-2 and WV15-3 contained gravels and could not be scanned for XRF or X-radiography. As such, for the locations associated with WV14-4 and WV14-5, carbon stocks in the lower sediments were included but were assumed to be zero in the other three locations.

Thiessen polygons (Thiessen, 1911; Goovaerts, 2000) were created in ArcGIS to appropriately apportion the carbon stock for each core across the area of the floodplain associated with the cores (Figure 3). The carbon stock for each core was multiplied by the area of the polygon. The areal carbon stocks were then summed to produce a total carbon stock for the whole floodplain.

The error associated with the carbon stock for each Thiessen polygon was calculated by multiplying the error by the area of the polygon. The total error for all cores was additively propagated.

The atypical setting of fine-grained, cohesive floodplain development within this upland environment is not limited to a few floodplains, but many that are associated with the catchments draining the localised blanket peat. Google Earth Pro was used to identify other floodplains in the River Ashop and Alport valleys with a similar floodplain-like morphology and further using the polygon tool, calculate the area of each of these floodplains (Figure 3). Floodplain boundaries were determined by the visual interpretation of the floodplain edges encroaching on the channel boundary from imagery. Sharp breaks of slope and changes in vegetation mark the floodplain boundaries in these constrained upland systems so that there is a high degree of confidence in floodplain definition. 57 floodplains were identified in total; 13 along the River Ashop, 31 along the River Alport and 13 after the confluence of these two rivers leading into Ladybower reservoir.

The depth of organic-containing sediment in the floodplain study site was approximately 1 m. To account for varying sediment depths of the identified floodplains, a field survey of a selection of these floodplains was undertaken. Sediments equivalent to the upper sediments in the Woodlands valley (fine sediment with organic layers above a unit of unbedded coarse sand and gravel) were observed at all sites and the depth of these sediments recorded in 32 stream sections. The average depth was 90 cm (n=32; SD= 25 cm), supporting the assertion that these floodplains are similar in nature and context.

Individual carbon stocks for each identified floodplain in the River Ashop and Alport catchments were derived using their respective areas, and the average carbon stock per m^2 of the sampled floodplain. Error bounds were applied to the calculation of these carbon stocks by considering the errors associated both from the carbon density from the Woodlands Valley floodplain (errors derived from the prediction of density and carbon content from the Itrax data), total years of floodplain accretion (derived from basal radiocarbon date error range), and floodplain depth (error derived as 2 SD of measured floodplain depths). These were used to calculate a minimum and maximum range for the carbon stock associated with total floodplain area in the wider catchments.

Dating

Pb content was established on thick organic layers within the stratigraphy from both the east and west point-bars. Six samples across two cores were taken where three distinctive Pb peaks occurred. These three Pb peaks were almost completely consistent throughout all cores, and provided an opportunity for cross-correlation to establish an approximate chronology for some of these layers. Basal organic beds were also chosen in most cores to identify a chronological boundary for the onset of organic deposition across the floodplain. Two samples were also taken in order to obtain more modern estimations of age. Finally, two large pieces of wood were removed to approximate radiocarbon activity on a different type of material, rather than being limited to bulk organics. Therefore, samples were chosen for age approximation based on correlating cores, obtaining basal and modern dates, and providing the greatest range of datable material possible in these cores.

Radiocarbon dating was completed by two different laboratories. Initially a piece of unidentified wood from WV14-5 at 1014-1015 mm was dated and calibrated by Beta Analytic Inc. using the IntCal13 calibration curve (Reimer *et al.,* 2013) with the 2 sigma ranges of the result reported. Twelve bulk organic samples and one wood sample were prepared to graphite and dated by the NERC radiocarbon facility in East Kilbride (Figure 4). Samples were pre-treated using HCl, KOH and acidified sodium chlorite where appropriate.

Six samples for IRSL analysis were collected from the exposed bank of the west point-bar close to the location of core WV17-3. Five were in a vertical sequence at depths of 150, 290, 470, 610 and 780 mm, and one sample was located approximately 10 m to the SE along the exposed section at a depth of 810 mm, representing the same stratigraphic horizon as the 780 mm depth sample. One modern sample was also extracted from the bed sediments. IRSL sample preparation and dating were undertaken at the University of Sheffield using a potassium feldspar single-grain post-IR IRSL approach as outlined by Rhodes (2015).

Sample preparation comprised sieving to separate the 180-212 µm fraction, HCl and H_2O_2 treatments to remove carbonate

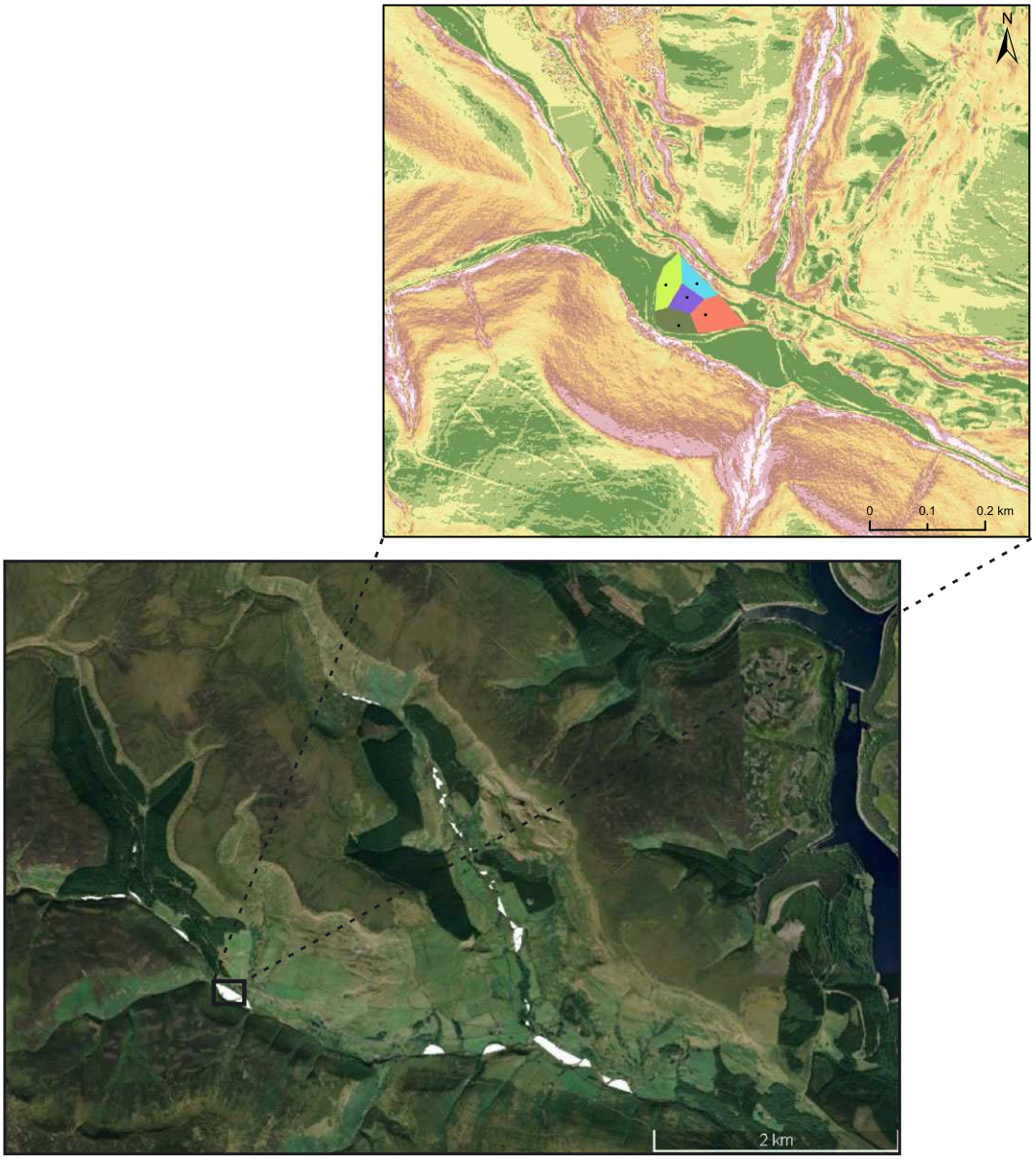

Figure 3. Thiessen polygons created from the division of the floodplain and distinguished by colour (upper) and identifiable small floodplains (white) in the River Ashop and Alport catchments. ©2018 Google. [Colour figure can be viewed at wileyonlinelibrary.com]

and organics respectively, density separation to isolate the K-feldspar fraction using sodium polytungstate at 2.58 g.cm^{-3}, then following copious rinsing, a brief 10% HF treatment to etch the surface of the grains. After rinsing and drying, sub-samples were sieved a second time to remove material <180 µm, and grains mounted individually in Risø single grain holders.

Measurements were made using a SAR (single aliquot regenerative-dose) protocol and a single grain post-IR IRSL approach (Brown *et al.,* 2015; Rhodes, 2015; Smedley *et al.,* 2015) within a Risø TL-DA-20 D DASH automated luminescence reader fitted with a BG3 and BG39 filter combination. IRSL stimulation (at 50 and 225°C) was with a 150 mW 830 nm IR laser at 90% power for 2.5 seconds incorporating a RG-780 filter within the single-grain attachment to reduce the resonance emission at 415 nm. Vishay TSFF 5210 870 nm IR diodes were used at 90% power for 40 seconds for a hot bleach treatment at 290°C at the end of each SAR cycle. A preheat of 250°C for 60 seconds was used, and signal growth was fitted with an exponential, or exponential plus linear, function.

Age estimation was based on the combination of the signals from the youngest apparent single grain ages for each sample (Rhodes, 2015). Dose rate contributions included in-situ NaI gamma spectrometer measurements of the gamma dose rate, with beta dose rate estimated on the basis of U, Th and K sediment concentrations determined using ICP-MS for U and Th and ICP-OES for K. An internal K content of 12.5% was assumed (Huntley and Baril, 1997), and cosmic dose rate was calculated based on sample depth. A uniform value of water content of 12.5 ± 2.5 was assumed based on measured water content results.

Results

Sedimentology

The cores were split into two facies types, indicating that two different processes may have formed the current day floodplain structure. The upper metre of sediments was characterised by interbedded organics and silty-sands, whereas, the lower sediments with the exception of WV14-4 and WV14-5 consisted of coarse sands and gravels with no visible bedding.

The sedimentology within the upper metre of the cores revealed a variety of sediment types including regular

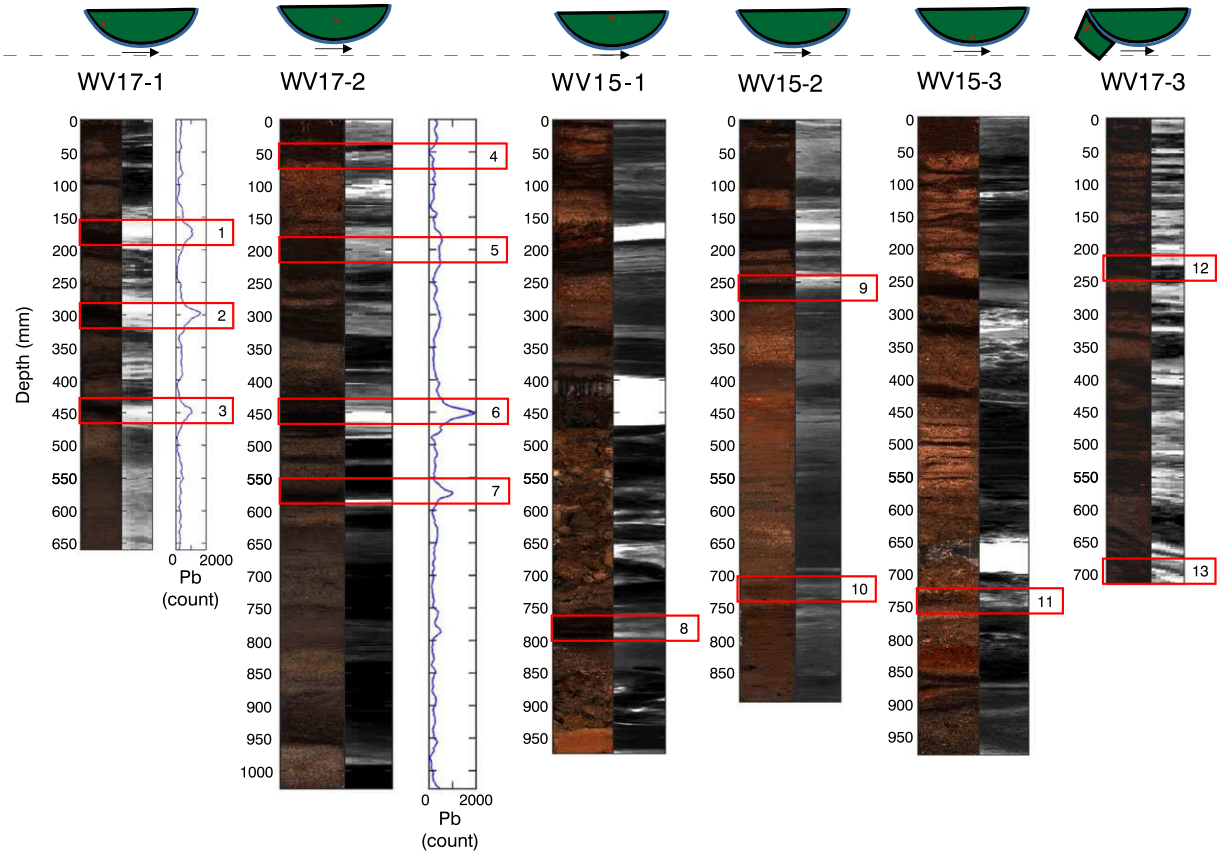

Figure 4. Compiled optical imagery and x-radiographic density determinations, in addition to Pb relative counts from ITRAX core scanning. Upper images represent relative core locations on the floodplain with arrows indicating direction of river flow. Red boxes highlight location of thirteen samples radiocarbon dated by NERC. All radiocarbon samples presented here were bulk soil with the exception of sample 10 which was unidentified wood. [Colour figure can be viewed at wileyonlinelibrary.com]

minerogenic layers with a variety of different oxidation states, organic layers, and mixed material containing both organics and minerogenic material. Detailed characterisation of the stratigraphy may be found in Alderson (2017). Key observable features have been identified (Figure 5).

Most cores had an over-thickened A horizon soil at the top of their profiles with alluvial parent material as observed by Daniels (2003). These organic A horizons were fairly fibrous, providing evidence for their recent growth and lack of decomposition.

Other organic layers in all cores displayed a variety of thicknesses and textures. In almost all organic layers, roots were still visible, although not in the same density as at the top of the cores. The presence of roots indicated that pedogenic processes had taken place within these layers. Organic banding tended to be thicker in all cores towards the top of the stratigraphy. Thin and occasionally discontinuous organic lenses within mineral sands were also observed in the same cores at a variety of depths. Organic layers in most cores had a fairly horizontal structure, with the exception of WV15-3 where the organic layers presented with an inclined structure indicative of microtopography on the floodplain surface.

Whereas the upper metre of most cores consisted of interbedded organic and mineral material, the lower sediments mainly consisted of coarse sands and gravels with little evidence of bedding. Only WV14-4 and WV14-5 had observable organics and are displayed in Figure 5.

Suspected flood couplets (Turner *et al.,* 2015) were observed in the fine-grained facies of all cores with some being linked to clearly observable grain-size changes and organic capping. At least four of these couplets were present in most cores indicating laterally extensive deposition.

Distinguishing the presence of allochthonous OM from sedimentology is challenging, as it may form the substrate (Baldwin *et al.,* 2013) for soil development, or may be trapped by rooted vegetation during a flood event (Gurnell, 2014). As such, it is plausible that within one organic profile, allochthonous material could be present at the bottom or top of a layer and subsequently mixed throughout via post-depositional processes. Therefore, the best opportunity for identifying distinct allochthonous layers was associated with thin layers or lenses which have been quickly enveloped by another flood event. Consequently, these events were more likely to be found towards the bottom of the core when the floodplain was not as high, so frequent inundation could take place. The most obvious thin layers were within WV15-3. Textural characteristics of the thin layers in all cores were difficult to observe as the layers were so thin (mm scale), but on observation there was no sign of roots.

Flood event stratigraphy

Direct measurement of grain size fractions through a flood event is a useful way to provide evidence for and understand the characteristics of a particular flood event (Schillereff *et al.,* 2014). Individual flood events may be assumed to end where the base of an organic bed begins by a sharp erosional contact (Törnqvist and van Dijk, 1993).

Grain size analysis was undertaken to provide further confidence on the sedimentological interpretation; that the distinctive mineral and organic couplets were associated with flood events (Figure 6). WV14-5 was chosen as the central core from the floodplain, characterised by clear minerogenic units with

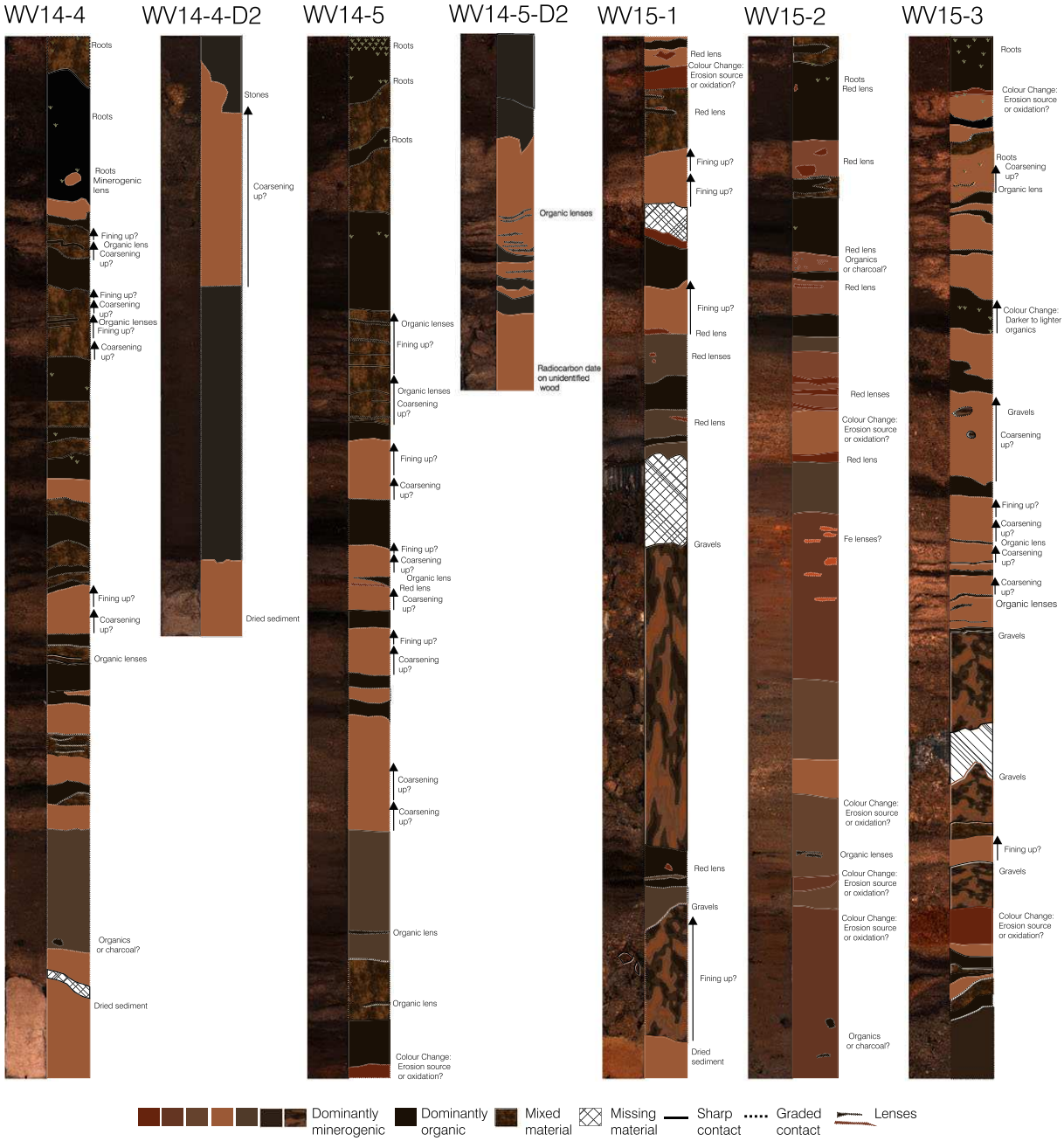

Figure 5. Optical imagery from ITRAX core scanning and interpretation of sedimentological features of the floodplain material. Scanned lower sediments (beyond 1 m) represented by D2, for drive 2. [Colour figure can be viewed at wileyonlinelibrary.com]

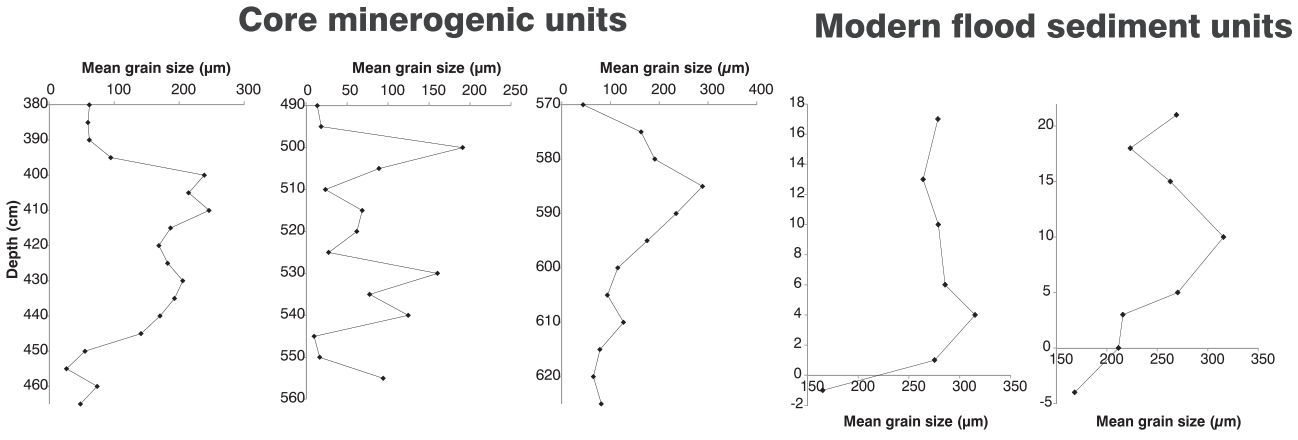

Figure 6. Mean grain size of three flood units in WV14-5 and two modern day sediment mounds from a large overbank flood event.

an organic capping, to investigate grain size relationships through suspected flood events, and through the organics on either side of the flood event. A discernible trend in mean grain size can be distinguished in two layers (380-465 mm and 570-625 mm). A coarsening upward sequence was distinguished with the coarsest grain size at 400 mm and 585 mm respectively, followed by a fining upwards sequence up to the top of the layer and partially into the organics. This sequence is in agreement with interpretation from Costa (1974) where the grain sizes coarsen up whilst flow velocity increases; with the maximum grain size representing the peak of the flood and the waning of the floodwaters represented by a fining upwards sequence.

The layer from 490 to 555 mm is more complex with two sequences of coarsening up and fining up. The first section fined up from 550 mm with the maximum mean grain size at 530 mm. The sequence then approximately fined upwards until 510 mm when coarsening upwards proceeded. The maximum mean grain size was at 500 mm followed by another fining up sequence. This minerogenic section was split by an organic lens, indicating that there were actually two separate flood events.

A modern overbank flood event provided the opportunity to validate the grain size relationships observed in the floodplain stratigraphy. Both samples of modern deposition, confirmed the coarsening up followed by fining up relationship (Figure 6). The combination of the modern and palaeo-grain size relationships give credence to the interpretation that the mineral-organic sequences were distinct flood events.

Core correlation

The identification of flood couplets and the horizontal structures of facies across the floodplain suggest that overbank deposition has occurred. However, the stratigraphy is complex and not all events may manifest in the same way or at all, spatially across the floodplain. If certain stratigraphic units can be linked, this gives further confidence that the upper metre of sediments in this floodplain have formed by vertical accretion as a result of overbank flood events.

Three distinctive Pb peaks were observed across most of the cores and have been cross-correlated in Figure 7. Absolute values of Pb were unimportant in comparison, because Pb is expressed in peak area (counts) and therefore absolute Pb values between cores were not comparable. These peaks were arguably most distinctive in WV14-4 and appeared to be associated with what are characterised according to the classification scheme as relatively thick, autochthonous organic layers. These three peaks form the basis of the inter-core correlation as demonstrated in Figure 7 and aid in interpreting the visual stratigraphy of the cores. These layers were selected for age approximation in WV17-1 and WV17-2, to confirm that the layers were correlated and to establish the age of the sediment containing the Pb.

One of the most notable differences between cores was the sedimentology of WV15-2, with the absence of organic layers below 300 mm. As this core is distal from the present channel, one could assume that it was unlikely that regular overbank deposition has occurred in the past, with the bulk of this material accreting by other processes such as lateral point-bar accretion. However, the presence of the cut-off channel indicated by the morphology of the floodplain and the fresh trash material observed, suggested that different processes may have occurred. In flood, high flows would cut off the meander flowing across the location of WV15-2. The lack of overbank fines and pedogenic development below 300 mm suggested that the floodplain was regularly inundated in this way, without time for pedogenesis to take place. An alternative explanation relates to a migrating channel over the lifetime of the floodplain. Although, the valley is relatively well constrained, there is evidence of a palaeochannel from topographic inspections of the floodplain, which could explain the predominance of mineral material at this location.

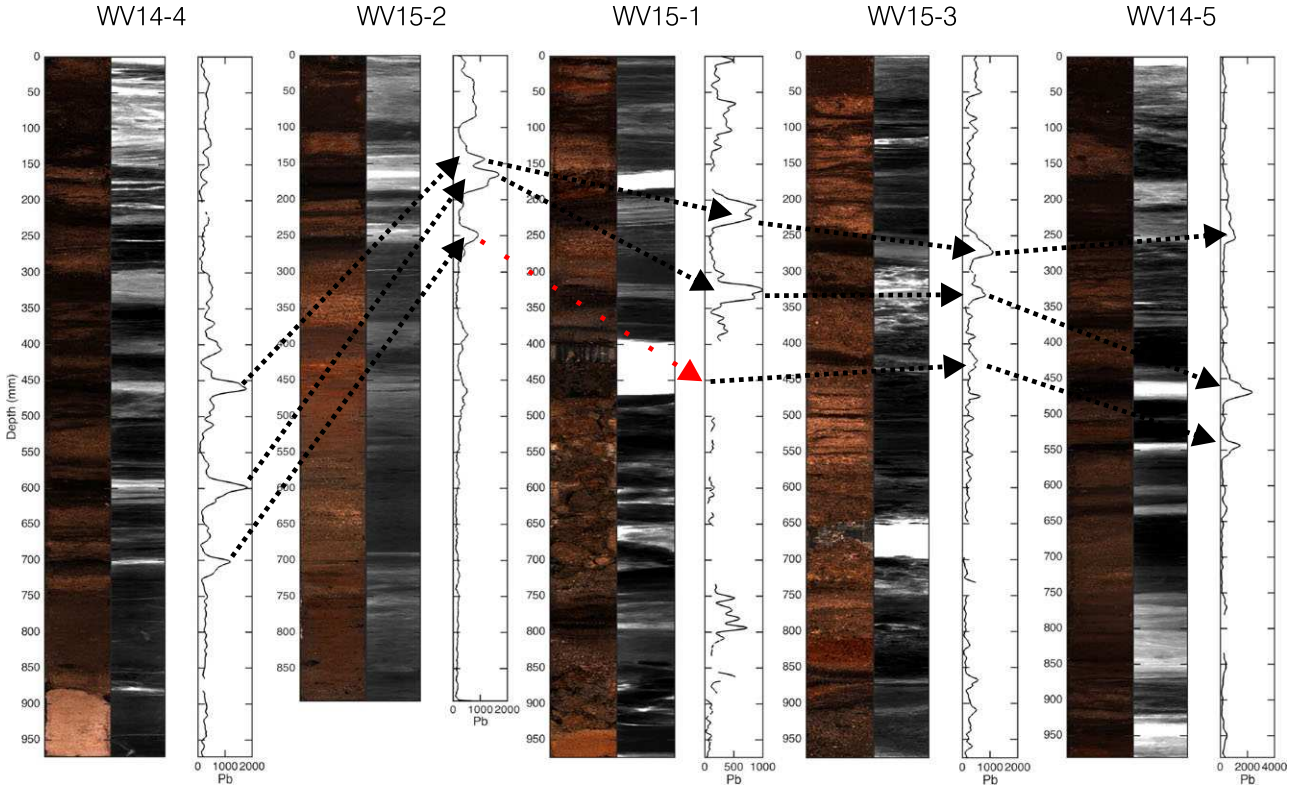

Figure 7. Pb peak correlations between coring locations. [Colour figure can be viewed at wileyonlinelibrary.com]

The core correlation linking Pb peaks clearly demonstrated that most of the floodplain development occurred by concurrent deposition with the exception of the most distal part of the floodplain relative to the present-day channel, where a cut-off channel or palaeochannel has influenced the sedimentology.

Age of floodplain

To aid the interpretation of the geomorphological formation and development of this floodplain, dating control on the floodplain stratigraphy was required.

The unidentified piece of wood at the base (1014-1015 mm) of the lower sediments of WV14-5 was dated by Beta Analytic as being between 500 to 310 Cal years BP. A second piece of wood towards the bottom of the upper metre of sediments of WV15-2 (730 mm) was dated at 333 ±37 years BP (Table II). These two ages suggested that the upper stratigraphy of the floodplain was circa 500 years old.

The bulk organic layers ranged from 1425 ±37 to 6043 ±38 years BP, with one sample dated as modern or late 1950s (Table II). The average age of the bulk organic ages excluding the modern age was 3010 years BP. Eight out of eleven bulk organic ages (excluding the modern sample) fit within 3000 years BP ±1000 years, with three outliers, two of which were slightly more extreme (1425 and 6043 years BP). Contrary to the interpretation of the sedimentology, these ages suggest that a substantial proportion of these thick organic layers were derived from the erosion of 'old' peat and that the overbank sediments observed in the first metre were formed in the last 500 years. An age depth model is therefore impossible to produce for the upper sediments, as the bulk organic layers are at least in part derived from elsewhere and contain a complex mixture of ages dependent on the age of the material from which they have been derived in the peatland catchment.

The IRSL dating samples were taken from the bank of the west point-bar as opposed to the samples for radiocarbon dating taken from both point-bars spanning the single meander bend (Figure 2). Around 50% of measured grains provided a finite age estimate, and these formed a wide range of measured apparent values in each case. The dominant effect producing this spread of apparent single grain ages is incomplete signal zeroing prior to deposition, although some samples also show indications of post-depositional mixing of younger material.

The ages excluding the modern sample range from 430 to 1430 years (Table III). A new basal sample was taken at 810 mm (WV16-01 – Shfd16076) following concerns about possible anthropogenic modifications of the floodplain affecting sample WV14-05 (Shfd15054), as this age appeared inverted in the stratigraphic column. Sample WV14-02 (Shfd15051) from a depth of 29 cm provides an anomalously high age estimate, and it is presumed that this deposit was laid down rapidly, possibly at night, with little opportunity for constituent grains to be bleached. The modern sample gives an age of 40 ±80 years, suggesting that at least some grains from this sample were reasonably well zeroed at this location.

The original basal sample (WV14-05 Shfd15054 at 78 cm depth) showed a mixture of zero age grains and older (c. 1,000 yr old) grains (Figure 8a), while the replacement sample (WV16-01 Shfd16076) showed no signs of grains younger than the combined age of 1060 ±110 years and provided additional confidence that the previous estimate was based on a contaminated location. This sediment sequence was deposited between 1000 and 400 years ago, and is therefore slightly older than the overbank deposition dated by ^{14}C in the adjacent

Table II. Radiocarbon dates provided by NERC laboratories. Samples taken from the east and west point-bars

Sample type	Publication code	Sample identifier	^{14}C Enrichment (% Modern ± 1 σ)	Conventional Radiocarbon Age (years BP ± 1 σ)	%Carbon Content	$\delta^{13}C_{VPDB}$‰ (± 0.1)
Bulk organic	SUERC-72209	WV17-1 180 mm	103.73 ± 0.47	N/A	20.0	-29.0
Bulk organic	SUERC-72210	WV17-1 300 mm	75.08 ± 0.34	2302 ± 37	26.3	-29.1
Bulk organic	SUERC-72211	WV17-1 460 mm	71.89 ± 0.33	2651 ± 37	11.4	-27.9
Bulk organic	SUERC-72219	WV17-2 30 mm	73.60 ± 0.34	2462 ±37	7.7	-28.2
Bulk organic	SUERC-72212	WV17-2 180 mm	83.74 ± 0.38	1425 ± 37	9.1	-27.8
Bulk organic	SUERC-72213	WV17-2 430 mm	74.11 ± 0.32	2407 ± 35	25.4	-28.0
Bulk organic	SUERC-72218	WV17-2 560 mm	70.63 ± 0.32	2793 ± 37	6.8	-27.6
Bulk organic	SUERC-72200	WV15-1-D1 900 mm	59.93 ± 0.26	4113 ± 35	1.8	-27.3
Bulk organic	SUERC-72201	WV15-2 250 mm	47.13 ± 0.22	6043 ± 38	2.1	-25.8
Wood	SUERC-72207	WV15-2 730 mm	95.94 ± 0.44	333 ± 37	38.1	-25.4
Bulk organic	SUERC-72202	WV15-3 770 mm	68.04 ± 0.31	3094 ± 37	21.0	-28.1
Bulk organic	SUERC- 72220	WV17-3 270 mm	68.03 ± 0.31	3094 ± 37	9.9	-28.2
Bulk organic	SUERC- 72221	WV17-3 720 mm	71.20 ± 0.31	2729 ± 35	7.7	-27.8

Table III. IRSL dating of west floodplain point-bar and channel-bar. Bold type indicative of data used to create an age-depth model

Field code	Laboratory code	Depth (m)	Stratigraphic notes	De (Gy)	1 σ uncertainty	Dose rate (mGy/a)	1 σ uncertainty	Age (years)	1 σ uncertainty
WV14-01	**Shfd15050**	**0.15**	**Main section**	**1.46**	**± 0.47**	**3.38**	**± 0.18**	**430**	**± 140**
WV14-02	Shfd15051	0.29	Main section	3.58	± 0.23	2.50	± 0.13	1430	± 120
WV14-03	**Shfd15052**	**0.47**	**Main section**	**1.98**	**± 0.17**	**2.36**	**± 0.11**	**840**	**± 90**
WV14-04	**Shfd15053**	**0.61**	**Main section**	**1.82**	**± 0.14**	**2.57**	**± 0.14**	**710**	**± 70**
WV14-05	Shfd15054	0.78	Main section	1.97	± 0.45	3.19	± 0.14	620	± 140
WV14-06	Shfd15055	0.15	Modern bar	0.08	± 0.18	2.24	± 0.17	40	± 80
WV16-01	**Shfd16076**	**0.81**	**Second section**	**2.89**	**± 0.28**	**2.73**	**± 0.11**	**1060**	**± 110**

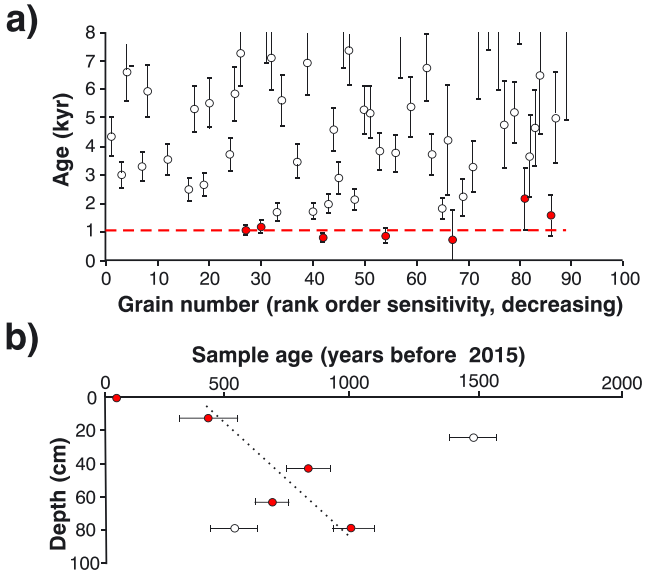

Figure 8. a) Variability in old basal sample (white, open circles) and new basal sample (red circles) b) Age-depth relationship of floodplain sediments based on IRSL dating. Red circles (with the exception of the modern date) used to create age-depth model. [Colour figure can be viewed at wileyonlinelibrary.com]

Table IV. Regression statistics for C and Inc/Coh ratio in addition to dry bulk density and radiographic greyscale correlations

	C	Density				
	WV14-5	WV14-4	WV14-5	WV15-1	WV15-2	WV15-3
R	0.868	0.830	0.714	0.618	0.460	0.369
R^2	0.753	0.689	0.510	0.382	0.212	0.136
p	<0.001	<0.001	<0.001	<0.000	0.041	0.120

point-bar. Including only those ages marked in bold in Table III produces the age-depth relationship shown by the dashed line in Figure 8b.

Carbon stocks and uncertainties

Carbon concentration and sediment density were derived from Itrax core scanning data using X-radiographic density and Inc/Coh as proxies. Regression analysis of direct measurements against the proxy data for a subset of samples are displayed in Table IV. The relationship between Inc/Coh and C% measured using a CHN analyser had a strong positive (0.75 R^2) significant relationship ($p<0.01$), and therefore gives us confidence that Inc/Coh represents a useful proxy for C%. Cores WV14-5, WV14-4 and WV15-1 had relatively strong positive relationships between average radiographic greyscale and dry bulk density which were significant ($p<0.01$). WV15-2 had a weak positive correlation which was significant ($p<0.05$). However, the relationship between radiographic greyscale and dry bulk density was much weaker in WV15-3 with a positive correlation that was not significant. Šidák corrections to alleviate the issue of multiple comparisons produced a confidence interval of 99% to test at, resulting in the correlations for WV15-2 and WV15-3 being not significant. Despite this, the correlations may still be used, as derived p values were not a measure of whether there was a physical relationship as it is well established that both proxies and the actual measures are related. The relationships between density in each core were clearly different (Figure 9) and therefore it was important to generate individual relationships.

Total carbon stocks are presented in Table V with their associated error. WV15-2 had the largest carbon stock followed by WV14-5, WV15-1, WV15-3 and finally WV14-4. The error associated with the carbon stocks was largest for WV14-4 and WV15-3 but was still within a reasonable range. The total stock in the floodplain was 325 ±10 tonnes.

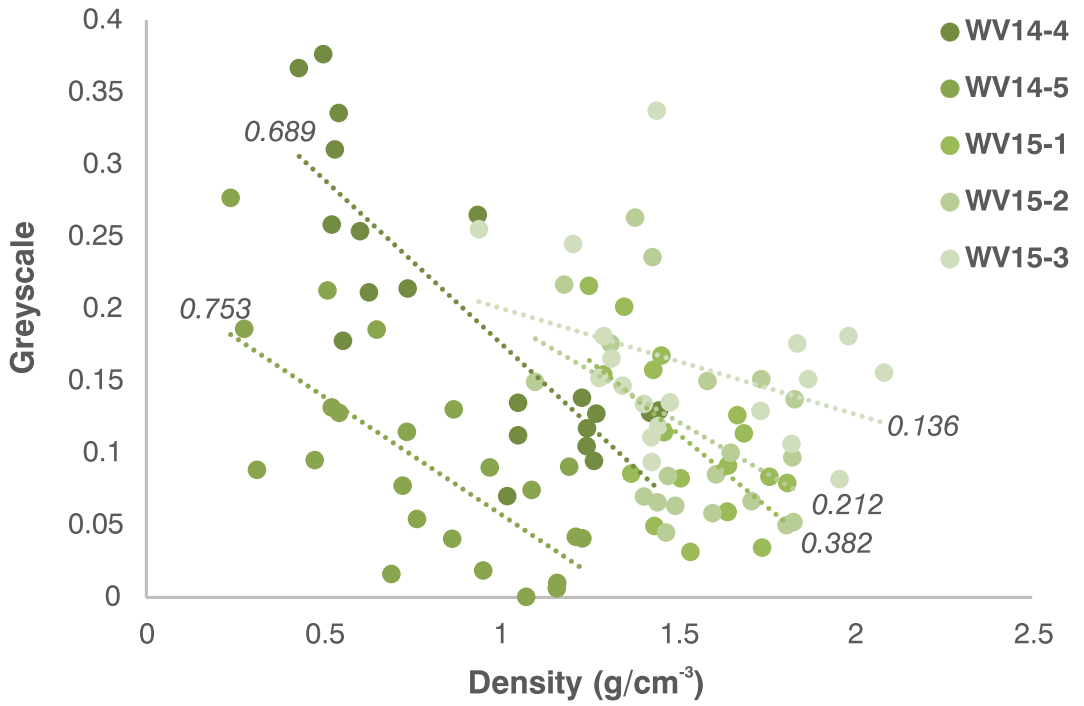

Figure 9. Radiograph and density relationships for each core. p values indicate significant values according to the Šidák correction. [Colour figure can be viewed at wileyonlinelibrary.com]

Table V. Total carbon stock per core and within floodplain

Core	Total carbon represented by core (kg m^{-3})	Area of Thiessen Polygon (m^2)	Total Carbon stock in Thiessen polygon (t)
WV14-4/WV17-1	45 ± 5	828	37 ± 4
WV14-5/WV17-2	59 ± 3	1769	105 ± 4
WV15-1	47 ± 1	1169	55 ± 0.9
WV15-2	97 ± 0	803	78 ± 0.1
WV15-3	35 ± 5	1506	50 ± 8
Total:	**283**	**6075**	**325 ± 10**

For the wider catchment, the most extensive floodplain development and hence the largest stocks by this extrapolation were below the confluence (Table VI), followed by the River Ashop and then the River Alport (associated with their areas). The total carbon stock for floodplains identifiable with the two catchments was between 3482 and 13460 tonnes, which represented a substantial stock of carbon in an area where floodplains are atypical.

This extrapolation of carbon stocks rested on the assumption that the WV floodplain is representative of the wider system. This was a substantial assumption, but was supported by the similar context and scale of these floodplains. Variations based on floodplain depth and carbon density variation within a single floodplain were considered by using minimum and maximum bounds. However, the OC content and the sourcing of OC within the extrapolated floodplains, in addition to floodplain area identification does represent an unknown error, although the similar context of the floodplains is reassuring. Uncertainties withstanding, the extrapolation was useful because it allowed comparison with existing understanding of the carbon budgets of the wider system in order to establish the significance of the data from a singular floodplain.

Carbon stock in context

If the Conventional Radiocarbon Age of the basal radiocarbon age estimate from WV14-5 D2 (500 to 310 Cal years BP) is used, (corrected for isotopic variations and an assumed delta ^{13}C), and the years of additional deposition from 1950 to 2016 are taken into account, we can estimate that the upper portion of the floodplain has accreted over 376-566 years. The total carbon stock for the Ashop and Alport valley floodplains calculated above, divided equally over these years equated to between 6.2-35.8 (best estimate: 17.7) t C yr^{-1}. The combined catchment area of the Rivers Ashop and Alport was 49 km^2. Therefore, the rate of accumulation per year was between 0.1-0.7- t C km^{-2} yr^{-1}. Data from a previous study has shown fluvial POC flux from the River Ashop near the study site estimated at 16.4 t C km^{-2} yr^{-1} (Pawson, 2008) which means that approximately between 0.8-4.5-% of the POC annual flux was stored. This POC flux was based on recent data and does not account for a variable flux over time. In fact, the POC flux is likely to be lower now than during the last 500 years, because of natural revegetation in the area (Crowe *et al.,* 2008). Large investments in artificial revegetation in the wider area have been shown to drive large reductions in POC flux by an order of magnitude (Alderson *et al.,* 2019). Higher POC fluxes during earlier stages of floodplain development would mean that floodplain carbon storage as a proportion of fluvial POC yield estimated here is a maximum amount.

Table VI. Floodplain carbon stocks in River Ashop and River Alport catchments

	Number	Area (m^2)	Carbon stock range (tonnes)
River Ashop	13	41640	844-3261
River Alport	31	33581	680-2630
After confluence	13	96615	1958-7568
Total	**57**	**171836**	**3482-13460**

Fluvial sediment taken during rising flood stages in the River Ashop catchment was on average 30% OC (Pawson, unpublished data). In comparison, average C% across the WV cores was 5%, with the possibility that deposited C has been largely oxidised (83% loss). Petrogenic carbon from this location is negligible (Shuttleworth *et al.,* 2015) so this cannot explain the discrepancy. An alternative explanation is that sorting of organic sediment has occurred during the flood event with the end product of OC deposited on the floodplain becoming diluted. However, supporting the former hypothesis, Evans *et al.* (2013) concluded 80% of POC exported from peatlands is eventually emitted as CO_2. Fluctuating water tables typical of these floodplain environments, are less conducive to preservation of OC than water saturated peatland environments, making oxidation of OC prevalent. Thus, using the more conservative estimate of 80% oxidation from Evans *et al.* (2013), floodplain carbon storage equivalent to 0.1-0.7 t C km^{-2} yr^{-1} equates to 0.6-3.7- t C km^{-2} yr^{-1} of original deposition. This further equates to between 3.8-22.3-% of the modern-day fluvial POC flux. Potential for in situ soil carbon accumulation means this is a maximum estimate.

Based on sedimentological interpretation identifiable organic layers may be apportioned by source (Figure 10). It is important to note that minerogenic carbon was classified as allochthonous carbon as it did not develop in-situ and predominantly mineral samples had very low C contents. The Millstone Grit geology in the catchment has a very low C% and there is little evidence of shales in the stratigraphy. The carbon stock was thus divided as 23% allochthonous and 77% autochthonous organics. This was clearly an underestimation of allochthonous organics as the derived radiocarbon ages showed that the bulk layers were much older than the floodplain itself and must be at least in part derived from eroded soils elsewhere in the catchment. These layers however were also clearly partially autochthonous as they feature roots and the consolidated texture associated with in-situ soil growth.

Discussion

Bringing together the variety of methodological approaches taken in this study, presents the opportunity to deduce how the floodplain formed and evolved, and the links between these processes and carbon sequestration. This further allows us to make inferences about floodplain development and carbon cycling in the wider catchment. We use the floodplain sedimentology and chronology to establish, and evaluate the timing of the formation of the floodplain and the OC stored within, in relation to other catchment events. Furthermore, information from other studies in the catchment is utilised to contextualise the role of the floodplains in processing laterally redistributed carbon.

Geomorphological evolution of the floodplain

The nature of the palaeochannel and the grain sizes at the bottom of the floodplains suggests that the basal sediments were probably formed by lateral accretion processes or as rapid

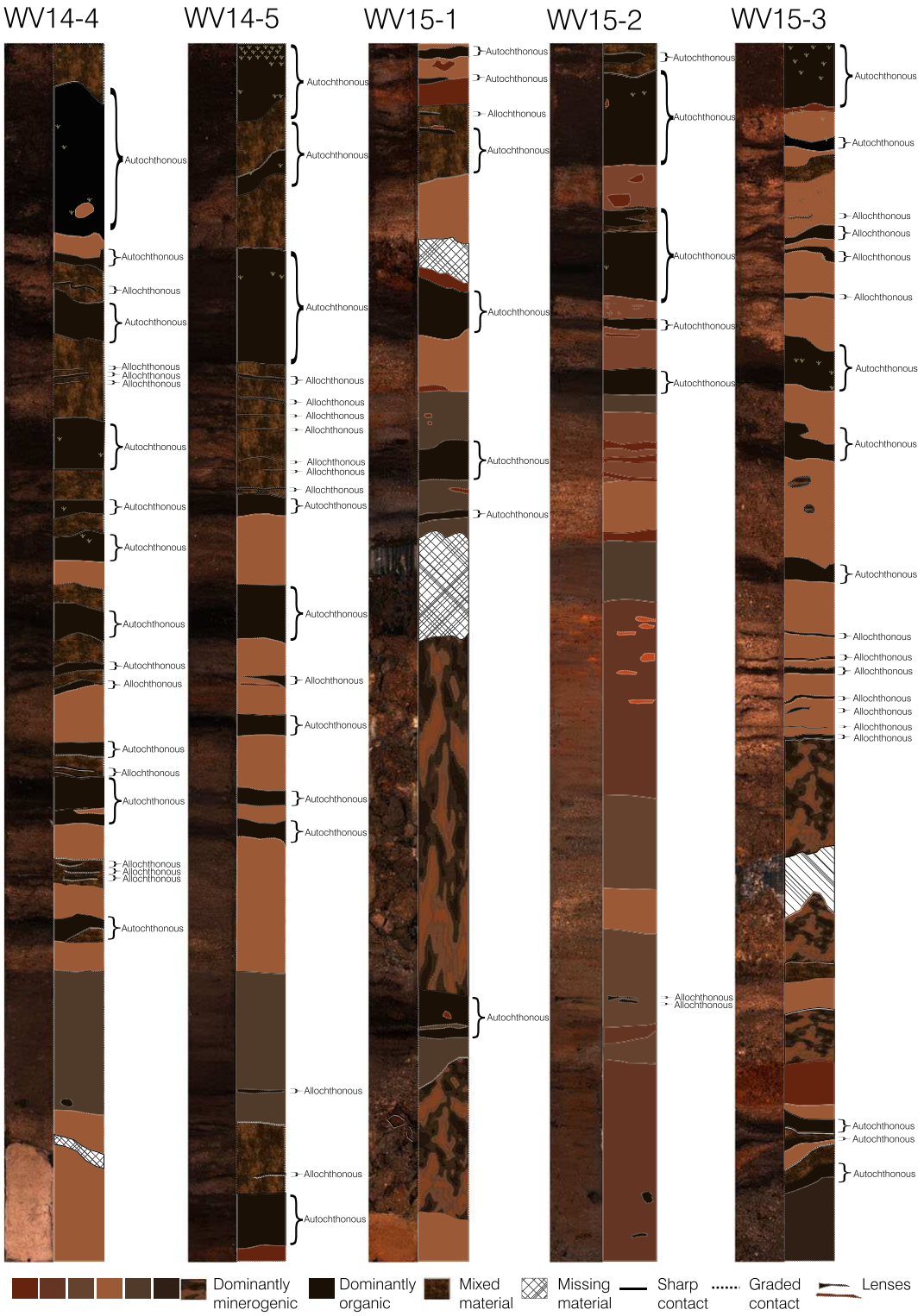

Figure 10. Characterising organics as allochthonous (33 layers) and autochthonous (40 layers) on the basis of sedimentology. [Colour figure can be viewed at wileyonlinelibrary.com]

accretion of coarse gravels during flood events in a mobile channel. The existence of horizontal layers of fine sediments (approximately upper m) throughout most of the cores, and the correlated layers containing Pb, supports overbank deposition as a key process that has formed the upper metre of the modern-day floodplain.

This floodplain can thus be classified as a polyphase floodplain, common in these types of deposits as the different sections represent the legacies of past flow regimes. The majority of the units in the floodplain may be classified as confined vertical-accretion sandy floodplains which is order A2 in the energy classification scheme by Nanson and Croke (1992). The floodplain is present in an upland confined valley and is formed largely of sand which overlies basal gravels. The confined nature of the valley functions in intensifying the erosional power of extreme flood events. Typically, this type of floodplain builds over hundreds to thousands of years and may be eroded down to its base by a series of large floods or a catastrophic flood, after which it reforms. These floodplains are thus unstable in nature as they are built up of non-cohesive material.

However, this floodplain is clearly atypical of this characterisation in that it has become cohesive as substantial organic

material is present, building up multiple buried soils throughout its history. Roots from pedogenesis have acted to bind layers together and a vegetated surface has trapped finer sediment over time, transforming the floodplain into a confined cohesive vertical-accretion floodplain, which is not part of the classification of Nanson and Croke (1992). There are limited studies on pedogenic development on floodplains subject to periodic flooding (Saint-Laurent *et al.,* 2008). However, the analysis of alluvial soils may aid in the understanding of the geomorphological development and dynamics of the river system, as soils and palaeosols indicate periods of stabilisation by the river, or in this case periods where the sediment load was highly organic.

Dating techniques confirmed the floodplain age as late Holocene on the basis of the two wood radiocarbon dates that infer that the upper portion of the east point-bar of the floodplain is approximately 500 years old (years before 2016). This wood has likely been derived from elsewhere in the catchment, but almost certainly not from the peatland itself, as trees have not grown on the peatland since before the onset of peat erosion dated at between 7500 to 5400 BP (Tallis and Switsur, 1991). The two point-bars are therefore likely to be diachronous. The upper sediment unit within the west point-bar although slightly older, is still contemporary in age, with predictions of the onset of peat erosion in the Peak District which are broadly concentrated in the last millennium (Evans and Lindsay, 2010).

This age of the upper section of the east point-bar of the floodplain composing of overbank fines and organics is consistent with estimations of the onset of peat erosion in this specific area of 500 ±250 years (Evans and Lindsay, 2010), collated from the work of Tallis (Tallis, 1994, 1995, 1998) as between 700 and 400 years BP. This confirms that the floodplain development occurred during a period of major peat erosion.

The bulk ^{14}C trapped in some of the thick organic layers was proven to be substantially older than the age of the upper metre of sediments. Fluvial conventional radiocarbon ages from Upper North Grain, one of the headwater catchments associated with the River Ashop (Evans *et al.,* 2013), range from 2140 to 3190 years BP (77-67 % modern ^{14}C).

Sedimentary floodplain ages demonstrate that the lower extremities of the overbank sediment sequence in the floodplain were concurrent with the initiation of peat erosion. Organic matter eroded from surficial peats at this time and deposited during early floodplain development would therefore be approximately 500 years younger than surficial peats eroded and deposited today. The process of gully incision is often swift (Evans and Warburton, 2007), exposing the complete peat profile as a source of eroded sediment. Therefore, although initially the age of eroded source material is close to 500 years BP it rapidly becomes a mixed sample across the full age range of the peat profile.

There are clear consistencies between the modern ages of riverine POC and the ages of sedimentary OC stored throughout the floodplain. These similarities are consistent with a fluvial POC load dominated by old peat transported as a result of extensive gully erosion. The mean age of the fluvial load (approximately 3000 years BP) is approximately half the estimated age of the eroding peatlands and is consistent with an organic load derived from erosion through the full depth of the peat profile. The old age of OC in the floodplain sediments is therefore consistent with the bulk of stored OC deriving from deposition of older peat eroded from the catchment. However, it is clear that pedogenesis has also occurred within these layers as evidenced by the substantial root density present.

Variation in apparent age of OC observed in the WV floodplain sediments is therefore likely to be a result of different levels of dilution by in-situ vegetation that has subsequently decomposed, meaning that all layers may not feature the same proportion of allochthonous versus autochthonous material.

Implications of POC deposition versus pedogenesis

Extensive peat erosion in the blanket bogs of Bleaklow Plateau and Kinder Scout has occurred over the last 500 ±250 years, forming widespread gully systems within the deep peat. The POC flux even recently is substantial as far down the catchment as the Woodlands Valley study site (16.4 t C km^{-2} yr^{-1}: Pawson, 2008), and as major restoration efforts have taken place in recent years which have been successful, we may assume by inference that the POC flux was previously higher.

If the initial sedimentological interpretation was used without knowledge of the radiocarbon ages, 23% of the OM stored in the floodplain sediment was associated with allochthonous deposition. Nevertheless, evidence from the bulk organic matter ^{14}C measurements for this floodplain demonstrates that this is a substantial underestimation of the amount of re-deposited peat that has been stored in these floodplain sediments. However, these thick layers cannot simply be classed as allochthonous as there is little doubt that there is a mixture of in-situ organics and redeposited peat as the thick organic layers have firmly established root systems, that would not be characteristic of re-deposited POC. As such, the sedimentological classification cannot be used with confidence to discriminate between allochthonous and autochthonous sources.

The implication of these results is that there has been a substantial lateral redistribution of terrestrial carbon. The disparity in organic content between high flow suspended sediments and preserved floodplain sediments and previous work on sediment preservation (Pawson *et al.,* 2008; Evans *et al.,* 2013) indicate that the extensive peatland erosion has generated carbon flux to the atmosphere due to oxidation on the floodplain surface. The implication is that these headwater floodplains, despite acting as sites of substantial allochthonous carbon sequestration and generation of additional storage of autochthonous OC, are also hotspots of allochthonous carbon turnover and important components of the sediment cascade.

The presence of consolidated, organic floodplains is atypical in an upland landscape. Floodplain formation in these systems appears to be related to two geomorphological events. Extensive early Holocene landslide deposits reduce local valley gradients but the analysis presented here demonstrates that floodplain formation was not initiated until the late Holocene, concurrent with the onset of rapid erosion of the organic soils of the headwaters of this system, which dramatically increased the sediment load (Figure 11). The landslide event is contingent, (sensu Simpson, 1963) creating the accommodation space for floodplain genesis higher in the catchment than might normally be the case. Floodplain formation however was triggered by immanent (sensu Simpson, 1963) sedimentological processes driven by upstream erosion.

The floodplains created in this environment are a function of the severity of the peatland erosion in this region, representing an end-member with regards to fluvial POC export. This process has led to substantial lateral terrestrial carbon cycling, with storage of aged carbon and hotspots of carbon turnover as key outcomes.

Comparison of the floodplain storage of the fluvial POC flux in this catchment (0.8-4.5%) to other studies is difficult, since most relevant studies involve landscape-scale catchments which do not consist of organic-dominated soils. Nevertheless, Worrall *et al.* (2018) estimated overbank storage as 2% in a study of the River Trent, UK, using estimates of the proportion of bankfull discharge to estimate overbank sedimentation.

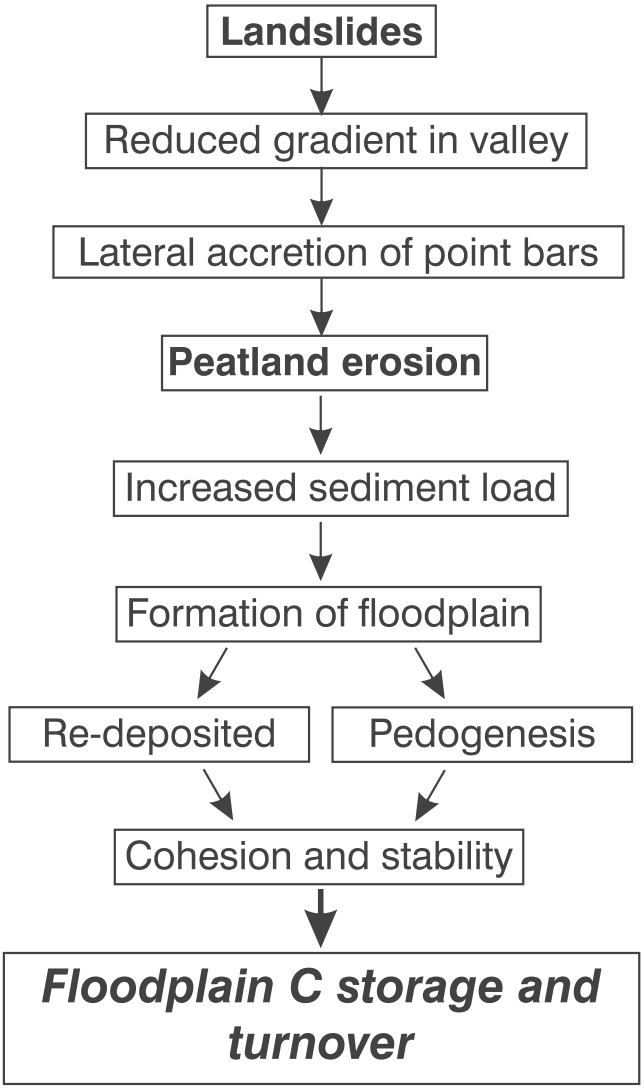

Figure 11. Processes leading to floodplain formation and carbon cycling in headwater catchments. The landslide process is contingent to this location, whereas the peatland erosion and the increased sediment load that follows are immanent processes.

Gomez *et al*. (2003) estimated that floodplain storage of the Waipaoa river in New Zealand was 4% of the annual POC flux. Similarities in the fluxes derived from these studies to the fluxes in this peatland dominated system are surprising. Highly organic fluvial sediment loads would suggest floodplain storage in organic-dominated catchments should be much higher than non-organic prevalent systems. The fact that in-situ preservation of carbon is at rates comparable to other floodplains is consistent with the hypothesis that significant oxidation of OC has occurred on the floodplain.

Although the formation of floodplains are a consequence of the extreme nature of this environment, the processes underlying topographic adjustment and erosion are inherent within upland landscapes. Severe erosion in particular is a threat in peatland environments that have up until now held an intact status, as a repercussion of climate and land use change. As such, continued enhancement of our knowledge of the role of floodplains in cycling and storing OC must become a critical research priority. Peatlands that are in the process of eroding, offer a unique opportunity to research floodplain development and carbon processing as it develops, rather than after the event.

As with erosion, deposition is an episodic event (Stallard, 1998) and understanding transient storage in river systems should become a research priority in terrestrial carbon cycling as increasing evidence demonstrates that these systems are not passive (for example Galy *et al.,* 2015; Hilton, 2016). In fact, these systems play an important role in setting the radiocarbon content (and organic matter quality) of riverine POC cycled back into the fluvial system and eventually the ocean, which models suggest may interrupt this pathway on timescales of millennia or greater (Torres *et al.,* 2017). Future research on previously severely eroded, and presently eroding systems must focus attention on the timescales of POC retention and the governing processes that dictate these timescales.

Conclusions

This is the first in-depth investigation of geomorphological history, carbon storage and carbon source in a floodplain from an organic headwater catchment. A unique approach using Itrax core scanning data was used to derive a carbon stock, suggesting that this method may prove successful in other locations and environments, without the need for time-consuming traditional methods.

The carbon stock estimate for the floodplains across the catchments is between 3482 and 13460 tonnes, equating to storage of between 0.8-4.5% of the modern-day fluvial flux, although this is almost certainly an overestimation as a result of restoration measures in the headwater catchments. Standard sedimentological approaches proved unreliable in

apportioning allochthonous/autochthonous carbon. ^{14}C aging of organic matter indicated a dominance of OC sourced from off-site erosion of peatlands. However, viewing these sites simply as carbon stored is misleading. Comparison of floodplain OC content with fluvial sediments indicates that these systems have potentially been turning over substantial quantities of carbon to the atmosphere.

Patterns of carbon flux have established that upland floodplains are an inherent part of this eroding peatland system. Storage and oxidation are both key processes with pedogenesis producing further carbon storage and stabilising the floodplain. In eroding peatland systems, erosion, deposition and turnover of carbon are intimately linked at the landscape scale and floodplains are a dynamic component of this system.

The role of headwater floodplains has not previously been recognised in terrestrial carbon cycling, but the work presented here suggests that they are a dynamic component of the terrestrial carbon cycle where net carbon sequestration is under the control of geomorphological as well as biological processes.

Further work is urgently required to ascertain the fate of floodplain carbon with regards to both quantity and quality. If headwater deposits are hotspots of carbon transformation, then erosional fluxes of POC from peatlands could be a source of atmospheric carbon. Understanding of the fluvial geomorphology and carbon cycling/storage status of floodplains as part of eroding upland catchments, may be central to estimation of the greenhouse gas balance of eroding peatlands.

Acknowledgements—The authors would like to thank the School of Environment, Education and Development at the University of Manchester for funding this research as part of a PhD studentship. The radiocarbon dating in this work was supported by the Natural Environment Research Council (NERC) Radiocarbon Facility NRCF010001 (allocation number 2034.1016.001). We would also like to thank the Geography laboratories staff at the University of Manchester (particularly John Moore and Thomas Bishop) for the access to and assistance with the Itrax core scanner, in addition to fieldwork assistance for this study. We would like to thank the National Trust for permissions to work on the field site. Finally, we would like to thank the two reviewers for their pertinent comments that have undoubtedly strengthened this paper.

References

Alderson, DM. 2017. The fate of carbon in upland floodplain sediments: a combined geomorphological and organic geochemical approach. PhD thesis, University of Manchester, Manchester. Available at: [https://www.research.manchester.ac.uk/portal/en/theses/the-fate-of-carbon-in-upland-floodplain-sediments-a-combined-geomorphological-and-organic-geochemical-approach(fb0b0de9-6906-4000-9d1d-897c382ca479).html] Accessed [08/02/2019]

Alderson DM, Evans MG, Shuttleworth EL, Pilkington M, Spencer T, Walker J, Allott TEH. 2019. Trajectories of ecosystem change in restored blanket peatlands. *Science of the Total Environment.* https://doi.org/10.1016/j.scitotenv.2019.02.095.

Aufdenkampe AK, Mayorga E, Raymond PA, Melack JM, Doney SC, Alin SR, Aalto RE, Yoo K. 2011. Riverine coupling of biogeochemical cycles between land, oceans, and atmosphere. *Frontiers in Ecology and the Environment* **9**(1): 53–60. https://doi.org/10.1890/100014.

Baldwin DS, Rees GN, Wilson JS, Colloff MJ, Whitworth KL, Pitman TL, Wallace TA. 2013. Provisioning of bioavailable carbon between the wet and dry phases in a semi-arid floodplain. *Oecologia* **172**(2): 539–550.

Battin TJ, Luyssaert S, Kaplan LA, Aufdenkampe AK, Richter A, Tranvik LJ. 2009. The boundless carbon cycle. *Nature Geoscience* **2**: 598–600. https://doi.org/10.1038/ngeo618.

Bonn A, Allott TEH, Evans M, Joosten H, Stoneman R (eds). 2016. *Peatland Restoration and Ecosystem Services*. Cambridge University Press: Cambridge.

Brown ND, Rhodes EJ, Antinao JL, McDonald EV. 2015. Single-grain post-IR IRSL signals of K-feldspars from alluvial fan deposits in Baja California Sur, Mexico. *Quaternary International* **362**: 132–138. https://doi.org/10.1016/j.quaint.2014.10.024.

Bullinger-Weber G, Le Bayon R-C, Thébault A, Schlaepfer R, Guenat C. 2014. Carbon storage and soil organic matter stabilisation in near-natural, restored and embanked Swiss floodplains. *Geoderma* **228-229**: 122–131. https://doi.org/10.1016/j.geoderma.2013.12.029.

Chawchai S, Kylander ME, Chabangborn A, Löwemark L, Wohlfarth B. 2016. Testing commonly used X-ray fluorescence core scanning-based proxies for organic-rich lake sediments and peat. *Boreas* **45**(1): 180–189. https://doi.org/10.1111/bor.12145.

Clark JM, Gallego-Sala AV, Allott TEH, Chapman SJ, Farewell T, Freeman C, House JI, Orr HG, Prentice IC, Smith P. 2010. Assessing the vulnerability of blanket peat to climate change using an ensemble of statistical bioclimatic envelope models. *Climate Research* **45**(1): 131–150. https://doi.org/10.3354/cr00929.

Cole JJ, Prairie YT, Caraco NF, McDowell WH, Tranvik LJ, Striegl RG, Duarte CM, Kortelainen P, Downing JA, Middelburg JJ, Melack J. 2007. Plumbing the global carbon cycle: integrating inland waters into the terrestrial carbon budget. *Ecosystems* **10**(1): 172–185. https://doi.org/10.1007/s10021-006-9013-8.

Costa JE. 1974. Stratigraphic, morphologic and pedologic evidence of large floods in humid environments. *Geology* **2**(6): 301–303. https://doi.org/10.1130/0091-7613(1974)2<301:SMAPEO>2.0.CO;2.

Costa JE. 1978. Holocene stratigraphy in flood frequency analysis. *Water Resources Research* **14**(4): 626–632. https://doi.org/10.1029/WR014i004p00626.

Croudace IW, Rindby A, Rothwell RG. 2006. ITRAX: description and evaluation of a new multi-function X-ray core scanner. *Geological Society, London, Special Publications* **267**: 51–63. https://doi.org/10.1144/GSL.SP.2006.267.01.04.

Croudace IW, Rothwell RG (eds). 2015. *Micro-XRF Studies of Sediment Cores: Applications of a non-destructive tool for the environmental sciences*. Dordrecht: Springer.

Crowe S, Evans MG, Allott TEH. 2008. Geomorphological controls on the re-vegetation of erosion gullies in blanket peat: implications for bog restoration. *Mires and Peat* **3**: 1–14.

Daniels JM. 2003. Floodplain aggradation and pedogenesis in a semi-arid environment. *Geomorphology* **56**(3-4): 225–242. https://doi.org/10.1016/S0169-555X(03)00153-3.

Duvauchelle P, Peix G, Babot D. 1999. Effective atomic number in the Rayleigh to Compton scattering ratio. *Nuclear Instruments and Methods in Physics Research B* **155**(3): 221–228. https://doi.org/10.1016/S0168-583X(99)00450-4.

Evans, C, Allott, T, Billett, M, Burden, A, Chapman, P, Dinsmore, K, Evans, M, Freeman, C, Goulsbra, C, Holden, J, Jones, D, Jones, T, Moody, C, Palmer, S and Worrall, F. 2013. Greenhouse gas emissions associated with non gaseous losses of carbon from peatlands- Fate of particulate and dissolved carbon. DEFRA project SP1205 Final report.

Evans M, Lindsay J. 2010. High resolution quantification of gully erosion in upland peatlands at the landscape scale. *Earth Surface Processes and Landforms* **35**(8): 876–886. https://doi.org/10.1002/esp.1918.

Evans M, Warburton J. 2005. Sediment budget for an eroding peat-moorland catchment in northern England. *Earth Surface Processes and Landforms* **30**(5): 557–577. https://doi.org/10.1002/esp.1153.

Evans M, Warburton J, Yang J. 2006. Eroding blanket peat catchments: Global and local implications of upland organic sediment budgets. *Geomorphology* **79**(1-2): 45–57. https://doi.org/10.1016/j.geomorph.2005.09.015.

Evans MG, Warburton J. 2007. *Geomorphology of upland peat: Erosion, form and landscape change*. Blackwell: Oxford.

Fortin D, Francus P, Gebhardt AC, Hahn A, Kliem P, Lisé-Pronovost A, Roychowdhury R, Labrie J, St-Onge G, PASADO Science Team. 2013. Destructive and non-destructive density determination: method comparison and evaluation from the Laguna Potrok Aike sedimentary record. *Quaternary Science Reviews* **71**: 147–153. https://doi.org/10.1016/j.quascirev.2012.08.024.

Francus P, Kanamaru K, Fortin D. 2015. Standardization and calibration of X-radiographs acquired with the ITRAX core scanner. In *Micro-*

XRF Studies of Sediment Cores: Applications of a non-destructive tool for the environmental sciences, Croudace IW, Rothwell RG (eds). Springer: Dordrecht; 491–505.

Galy V, Peucker-Ehrenbrink B, Eglinton T. 2015. Global carbon export from the terrestrial biosphere controlled by erosion. *Nature* **521**: 204–207. https://doi.org/10.1038/nature14400.

Gomez B, Trustum NA, Hicks DM, Rogers KM, Page MJ, Tate KR. 2003. Production, storage, and output of particulate organic carbon: Waipaoa River basin, New Zealand. *Water Resources Research* **39**(6): 1161. https://doi.org/10.1029/2002WR001619.

Goovaerts P. 2000. Geostatistical approaches for incorporating elevation into the spatial interpolation of rainfall. *Journal of Hydrology* **228**(1-2): 113–129.

Gurnell A. 2014. Plants as river system engineers. *Earth Surface Processes and Landforms* **39**: 4–25. https://doi.org/10.1002/esp.3397.

Hilton RG. 2016. Climate regulates the erosional carbon export from the terrestrial biosphere. *Geomorphology* **277**: 118–132. https://doi.org/10.1016/j.geomorph.2016.03.028.

Hoffmann T, Glatzel S, Dikau R. 2009. A carbon storage perspective on alluvial sediment storage in the Rhine catchment. *Geomorphology* **108**(1-2): 127–137. https://doi.org/10.1016/j.geomorph.2007.11.015.

Hoffmann T, Mudd SM, van Oost K, Verstraeten G, Erkens G, Lang A, Middelkoop H, Boyle J, Kaplan JO, Willenbring J, Aalto R. 2013. Short communication: Humans and the missing C-sink: erosion and burial of soil carbon through time. *Earth Surface Dynamics* **1**: 45–52. https://doi.org/10.5194/esurf-1-45-2013.

Holden J, Shotbolt L, Bonn A, Burt TP, Chapman PJ, Dougill AJ, Fraser EDG, Hubacek K, Irvine B, Kirkby MJ, Reed MS, Prell C, Stagl S, Stringer LC, Turner A, Worrall F. 2007. Environmental change in moorland landscapes. *Earth-Science Reviews* **82**(1-2): 75–100. https://doi.org/10.1016/j.earscirev.2007.01.003.

Huntley DJ, Baril M. 1997. The K content of the K-feldspar being measured in optical dating or in thermoluminescence dating. *Ancient TL* **15**: 11–13.

Jain V, Fryirs K, Brierley G. 2008. Where do floodplains begin? The role of total stream power and longitudinal profile form on floodplain initiation processes. *Geological Society of America Bulletin* **120**(1-2): 127–141. https://doi.org/10.1130/B26092.1.

Johnson RH, Walthall S. 1979. The Longdendale landslides. *Geological Journal* **14**(2): 135–158. https://doi.org/10.1002/gj.3350140211.

Lee JA, Tallis JH. 1973. Regional and Historical Aspects of Lead Pollution in Britain. *Nature* **245**: 216–218. https://doi.org/10.1038/245216a0.

Li P, Holden J, Irvine B, Mu X. 2017. Erosion of Northern Hemisphere blanket peatlands under 21st-century climate change. *Geophysical Research Letters* **44**: 3615–3623. https://doi.org/10.1002/2017GL072590.

Liu X, Colman SM, Brown ET, Minor EC, Li H. 2013. Estimation of carbonate, total organic carbon, and biogenic silica content by FTIR and XRF techniques in lacustrine sediments. *Journal of Paleolimnology* **50**: 387–398. https://doi.org/10.1007/s10933-013-9733-7.

Livett EA, Lee JA, Tallis JH. 1979. Lead, zinc and copper analyses of British blanket peats. *Journal of Ecology* **67**: 865–891. https://doi.org/10.2307/2259219.

Nanson GC, Croke JC. 1992. A genetic classification of floodplains. *Geomorphology* **4**(6): 459–486.

Pawson RR. 2008. *Assessing the role of particulates fluvial in the fluvial organic carbon flux peatland from eroding peatland systems*. University of Manchester.

Pawson RR, Evans MG, Allott TEH. 2012. Fluvial carbon flux from headwater peatland streams: Significance of particulate carbon flux. *Earth Surface Processes and Landforms* **37**(11): 1203–1212. https://doi.org/10.1002/esp.3257.

Pawson RR, Lord DR, Evans MG, Allott TEH. 2008. Fluvial organic carbon flux from an eroding peatland catchment, southern Pennines, UK. *Hydrology and Earth System Science* **12**: 625–634. https://doi.org/10.5194/hess-12-625-2008.

Pizzuto JE, Moody JA, Meade RH. 2008. Anatomy and dynamics of a floodplain, Powder River, Montana, U.S.A. *Journal of Sedimentary Research* **78**(1): 16–28. https://doi.org/10.2110/jsr.2008.005.

Reimer PJ, Bard E, Bayliss A, Beck JW, Blackwell PG, Bronk Ramsey C, Buck CE, Cheng H, Edwards RL, Friedrich M, Grootes PM, Guilderson TP, Haflidason H, Hajdas I, Hatté C, Heaton TJ, Hoffmann DL, Hogg AG, Hughen KA, Kaiser KF, Kromer B, Manning SW, Niu M, Reimer RW, Richards DA, Scott EM, Southon JR, Staff RA, Turney CSM, van der Plicht J. 2013. IntCal13 and Marine13 radiocarbon age calibration curves 0–50,000 years cal BP. *Radiocarbon* **55**(4): 1869–1887.

Rhodes EJ. 2015. Dating sediments using potassium feldspar single-grain IRSL: Initial methodological considerations. *Quaternary International* **362**: 14–22. https://doi.org/10.1016/j.quaint.2014.12.012.

Saint-Laurent D, Paradis R, Drouin A, Gervais-Beaulac V. 2016. Impacts of floods on organic carbon concentrations in alluvial soils along hydrological gradients using a Digital Elevation Model (DEM). *Water* **8**: 1–17. https://doi.org/10.3390/w8050208.

Saint-Laurent D, St-Laurent J, Lavoie L, Ghaleb B. 2008. Use geopedological methods for the evaluation of sedimentation rates on river floodplains, southern Québec, Canada. *Catena* **73**(3): 321–337. https://doi.org/10.1016/j.catena.2007.12.004.

Schillereff DN, Chiverrell RC, Macdonald N, Hooke JM. 2014. Flood stratigraphies in lake sediments: A review. *Earth-Science Reviews* **135**: 17–37. https://doi.org/10.1016/j.earscirev.2014.03.011.

Settele J, Scholes R, Betts R, Bunn S, Leadley P, Nepstad D, Overpeck JT, Taboada MA. 2014. In *Terrestrial and inland water systems. In: Climate Change 2014: Impacts,Adaptation, and Vulnerability. Part A: Global and Sectoral Aspects. Contribution of Working Group II to the Fifth Assessment Report of the Intergovernmental Panel on Climate Change*, Field CB, Barros VR, Dokken DJ, Mach KJ, Mastrandrea MD, Bilir TE, Chatterjee M, Ebi KL, Estrada YO, Genova RC, Girma B, Kissel ES, Levy AN, MacCracken S, Mastrandrea PR, White LL (eds). Cambridge University Press: Cambridge, United Kingdom and New York, NY, USA; 271–359.

Shuttleworth EL, Evans MG, Hutchinson SM, Rothwell JJ. 2015. Peatland restoration: Controls on sediment production and reductions in carbon and pollutant export. *Earth Surface Processes and Landforms* **40**(4): 459–472. https://doi.org/10.1002/esp.3645.

Simpson GG. 1963. Historical science. In *The Fabric of Geology*, Albritton CC (ed). Addison-Wesley, Reading; 24–48.

Smedley RK, Duller GAT, Roberts HM. 2015. Bleaching of the post-IR IRSL signal from individual grains of K-feldspar: Implications for single-grain dating. *Radiation Measurements* **79**: 33–42. https://doi.org/10.1016/j.radmeas.2015.06.003.

Stallard RF. 1998. Terrestrial sedimentation and the carbon cycle: coupling weather and erosion to carbon burial. *Global Biogeochemical Cycles* **12**: 231–257. https://doi.org/10.1029/98GB00741.

St-Onge G, Mulder T, Francus P, Long B. 2007. In *Continuous physical properties of cored marine sediments*, Hillaire-Marcel C, De Vernal A (eds), Vol. **1**. Elsevier. Developments in Marine Geology; 63–98.

Tallis JH. 1994. Pool-and-hummock patterning in a southern Pennine blanket mire II. The formation and erosion of the pool system. *Journal of Ecology* **82**(4): 789–803. https://doi.org/10.2307/2261444.

Tallis JH. 1995. Climate and erosion signals in British blanket peats: The significance of Racomitrium lanuginosum remains. *Journal of Ecology* **83**(6): 1021–1030. https://doi.org/10.2307/2261183.

Tallis JH. 1998. Growth and degradation of British and Irish blanket mires. *Environmental Reviews* **6**(2): 81–122. https://doi.org/10.1139/a98-006.

Tallis JH, Johnson RH. 1980. In *The dating of landslides in Longdendale, north Derbyshire, using pollen-analytical techniques*, Cullingford RA, Davidson DA, Lewin J (eds). Timescales in Geomorphology: Chichester, Wiley; 189–205.

Tallis JH, Switsur VR. 1991. Forest and moorland in the South Pennine uplands in the Mid-Flandrian period: I. Macrofossil evidence of the former forest cover. *The Journal of Ecology* **71**(2): 585–600. https://doi.org/10.2307/2259736.

Thiessen AH. 1911. Precipitation averages for large areas. *Monthly Weather Review* **39**(7): 1082–1084.

Thomson J, Croudace IW, Rothwell RG. 2006. A geochemical application of the ITRAX scanner to a sediment core containing eastern Mediterranean sapropel units. In *New Techniques in Sediment Core Analysis*, Croudace IW, Rothwell RG (eds). The Geological Society of London: London; 65–77.

Törnqvist TE, van Dijk GJ. 1993. Optimizing sampling strategy for radiocarbon dating of Holocene fluvial systems in a vertically aggrading setting. *Boreas* **22**: 129–145. https://doi.org/10.1111/j.1502-3885.1993.tb00172.x.

Torres MA, Limaye AB, Ganti V, Lamb MP, West AJ, Fischer WW. 2017. Model predictions of long-lived storage of organic carbon in river deposits. *Earth Surface Dynamics* **5**: 711–730. https://doi.org/10.5194/esurf-5-711-2017.

Tranvik LJ, Downing JA, Cotner JB, Loiselle SA, Striegl RG, Ballatore TJ, Dillon P, Finlay K, Fortino K, Knoll LB, Kortelainen PL, Kutser T, Larsen S, Laurion I, Leech DM, Mccallister SL, McKnight DM, Melack JM, Overholt E, Porter JA, Prairie Y, Renwick WH, Roland F, Sherman BS, Schindler DW, Sobek S, Tremblay A, Vanni MJ, Verschoor AM, Wachenfeldt E, Von and Weyhenmeyer, GA. 2009. Lakes and reservoirs as regulators of carbon cycling and climate. *Limnology and Oceanography* **54**(6): 2298–2314. https://doi.org/10.4319/lo.2009.54.6_part_2.2298.

Turner JN, Jones AF, Brewer PA, Macklin MG, Rassner SM. 2015. Micro-XRF Applications in Fluvial Sedimentary Environments of Britain and Ireland: Progress and Prospects. In *Micro-XRF Studies of Sediment Cores: Applications of a non-destructive tool for the environmental sciences*, Croudace IW, Rothwell RG (eds), Vol. **17**, Developments in Paleoenvironmental Research Vol. The Geological Society of London: London; 227–265.

Wolverson-Cope F. 1976. *Geology explained in the Peak District*. Scarthin Books: Devon.

Worrall F, Burt TP, Howden NJK, Hancock GR, Wainwright J. 2018. The fate of suspended sediment and particulate organic carbon in transit through the channels of a river catchment. *Hydrological Processes* **32**: 146–159. https://doi.org/10.1002/hyp.11413.

Worrall F, Evans MG, Bonn A, Reed MS, Chapman D, Holden J. 2009. Can carbon offsetting pay for upland ecological restoration? *The Science of the Total Environment* **408**(1): 26–36. https://doi.org/10.1016/j.scitotenv.2009.09.022.

Zehetner F, Lair GJ, Gerzabek MH. 2009. Rapid carbon accretion and organic matter pool stabilization in riverine floodplain soils. *Global Biogeochemical Cycles* **23**(4): 1–7. https://doi.org/10.1029/2009GB003481.

Zocatelli R, Moreira-Turcq P, Bernardes M, Turcq B, Cordeiro RC, Gogo S, Disnar JR, Boussafir M. 2013. Sedimentary evidence of soil organic matter input to the Curuai Amazonian floodplain. *Organic Geochemistry* **63**: 40–47. https://doi.org/10.1016/j.orggeochem.2013.08.004.